Myostatin is a negative regulator of adult neurogenesis in zebrafish

[#]Vishnu Muraleedharan Saraswathy[1,2], [#]Lili Zhou[1,2], Brooke Burris[1,2], Deepika Dogra[3,4], Sven Reischauer[3,5,6], and Mayssa H. Mokalled[1,2,7]

[#] Co-authors

[1] Department of Developmental Biology
Washington University School of Medicine, St. Louis, MO, USA 63110.

[2] Center of Regenerative Medicine
Washington University School of Medicine, St. Louis, MO, USA 63110.

[3] Department of Developmental Genetics, Max Planck Institute for Heart and Lung Research, Bad Nauheim 61231, Germany

[4] Department of Medical Genetics, Cumming School of Medicine, University of Calgary, Calgary, AB T2N 4N1, Canada

[5] Medical Clinic I, (Cardiology/Angiology) and Campus Kerckhoff, Justus-Liebig University, Giessen, 35392 Giessen, Germany.

[6] The Cardio-Pulmonary Institute, Frankfurt, Germany.

[7] Author for correspondence: *mmokalled@wustl.edu*

ABSTRACT

Intrinsic and extrinsic inhibition of axonal and neuronal regeneration obstruct spinal cord (SC) repair in mammals. In contrast, adult zebrafish achieve functional recovery after SC damage. While studies of innate SC regeneration have focused on axon regrowth as a primary repair mechanism, how local neurogenesis impacts functional recovery is unknown. We uncovered dynamic expression of *myostatin b* (*mstnb*) in a niche of dorsal ependymal progenitors after complete SC transection in zebrafish. Genetic loss-of-function in *mstnb* impaired functional recovery, although glial and axonal bridging across the lesion were unaffected. Using a series of transgenic reporter lines, we quantified the numbers of stem, progenitor, and neuronal cells in the absence of *mstnb*. We found neural stem cell proliferation was reduced, while newborn neurons were increased in *mstnb* null tissues, suggesting *mstnb* is a negative regulator of neurogenesis. Molecularly, neuron differentiation genes were upregulated, while the neural stem cell maintenance gene *fgf1b* was downregulated in *mstnb* mutants. Finally, we show that human FGF1 treatment rescued neuronal gene expression in *mstnb* mutants. These studies uncover unanticipated neurogenic functions for *mstnb* in adult zebrafish, and establish the importance of local neurogenesis for functional SC repair.

INTRODUCTION

Traumatic spinal cord injury (SCI) causes irreversible neuronal and systemic deficits (Hachem et al., 2017; Silva et al., 2014; Singh et al., 2014). In mammals, axon regrowth and neurogenesis are impeded by intrinsic and extrinsic inhibitory mechanisms that obstruct spinal cord (SC) regeneration (Alizadeh et al., 2019; Oyinbo, 2011; Sofroniew, 2018; Tran et al., 2021). Although multiple cell types including astrocytes and oligodendrocyte progenitor cells proliferate after SCI, the mammalian SC is incapable of generating mature neurons *in vivo* (Horky et al., 2006; Horner et al., 2000; Yamamoto et al., 2001). In contrast with mammals, highly regenerative vertebrates including teleost fish spontaneously recover after SCI. Following complete transection of SC tissues, adult zebrafish extend glial and axonal bridges across the lesion and achieve functional recovery within 6 to 8 weeks of injury. In addition to axon regrowth from hindbrain neurons, zebrafish regenerate motor neurons and interneurons around the lesion site (Becker et al., 1998; Becker et al., 1997; Kuscha et al., 2012a; Mokalled et al., 2016; Reimer et al., 2008). Yet, the contribution of local neurogenesis to functional recovery and the mechanisms that coordinate the regeneration of different neuronal subtypes remain to be determined.

Ependymal radial glial cells (ERGs) line the brain ventricles and SC central canal. ERGs co-express astroglial (*gfap* and *blbp*) and progenitor (*sox2* and *hey*) cell markers, and comprise populations of neurogenic stem cells in adult zebrafish (Kroehne et al., 2011; März et al., 2010; Ogai et al., 2014; Reimer et al., 2009; Than-Trong et al., 2020; Than-Trong et al., 2018). In uninjured neural tissues, the majority of ERGs are non-dividing, quiescent cells that possess epithelial-like features (Barbosa et al., 2015; Chapouton et al., 2010; März et al., 2010). Following brain and SC damage, ERGs undergo widespread proliferation and are thought to act as a major source of regenerated neurons (Adolf et al., 2006; Barbosa et al., 2015; Grandel et al., 2006; Kroehne et al., 2011). Activated ERGs undergo 3 modes of cell division: 1) symmetric division into ERGs, 2) asymmetric division into ERG and neural progenitors, or 3) symmetric division to generate differentiated neurons (Barbosa et al., 2015; Rothenaigner et al., 2011). Distinct lineage-restricted ERG domains emerge during SC regeneration in zebrafish. ERGs within the progenitor motor neuron (pMN) domain express *olig2* and generate *isl1/2*$^{+}$ and *hb9*$^{+}$ motor neurons after SCI (Reimer et al., 2008). On the dorsal and ventral sides of the pMN, ERGs give rise to *vsx1*$^{+}$ V2 interneurons and serotonergic neurons, respectively (Barreiro-Iglesias et al., 2015; Kuscha et al., 2012b). We recently showed that ventral ERGs undergo epithelial-to-mesenchymal transition (EMT), and that EMT is required for glial bridging and functional regeneration (Klatt Shaw et al.,

2021). Thus, despite their morphological similarities, ERGs elicit compartmentalized injury responses and proliferate into lineage-restricted progenitors during SC regeneration.

Myostatin (Mstn), also known as Growth differentiation factor 8 (Gdf8), is a Tgf-β superfamily member. Upon binding Activin type 2 and type 1 receptors, Mstn induces the phosphorylation and nuclear translocation of Smad 2/3 to regulate target gene expression (Massagué, 2012; Sartori et al., 2014; Sharma et al., 2015). Spontaneous and targeted Mstn loss-of-function mutations lead to double muscle phenotypes in zebrafish, mice, cattle and humans (Dogra et al., 2017; Kambadur et al., 1997; Schuelke et al., 2004; Whittemore et al., 2003). Mechanistically, Mstn controls lineage progression within myogenic stem cells (satellite cells) and progenitor cells (myoblasts). During muscle development, Mstn inhibits myoblast differentiation via negative regulation of the myogenic transcription factors MyoD and Myogenin. Mstn also suppresses satellite cell proliferation, differentiation, and muscle regeneration (Langley et al., 2002; McCroskery et al., 2003; McCroskery et al., 2005). However, it remains unclear whether recombinant MSTN proteins inhibit or stimulate myoblast proliferation (Rodgers et al., 2014; Taylor et al., 2001). Equally conflicting effects were reported for recombinant MSTN proteins on neuronal proliferation and neurite outgrowth *in vitro* (Kerrison et al., 2005; Wu et al., 2003), suggesting Mstn functions are dose- and context-dependent and that *in vivo* studies are required to decipher the role of Mstn in the nervous system.

Tgf-β signaling directs immune, fibrotic, or regenerative injury responses across tissues and species. As zebrafish SCs regenerate without fibrotic scarring, we postulated that Tgf-β signaling is pro-regenerative in adult zebrafish. By surveying the expression of Tgf-β ligands after SCI, we found *mstnb* is induced in dorsal ERGs of lesioned SC tissues. *mstnb* mutants showed normal baseline swim capacity but failed to achieve functional recovery following SCI, despite having normal axonal and glial bridging across the lesion. Mstnb inhibition using genetic loss-of-function and pharmacological approaches enhanced neurogenesis and diminished ERG proliferation. A series of transgenic reporter lines was used to quantify the numbers of neural stem cells (NSCs), intermediate neural progenitors (iNPs), and interneurons. These studies revealed NSC proliferation was reduced, while regenerating neurons were increased in *mstnb* mutants. RNA sequencing showed neuron differentiation genes were upregulated in *mstnb* mutants. Finally, we show that the neural stem cell maintenance gene *fgf1b* was downregulated in *mstnb* mutants, and that human FGF1 treatment rescued neuronal gene expression. These studies indicate that *mstnb* acts as an essential negative regulator of adult neurogenesis in zebrafish, and that injury-

induced *mstnb* expression is required to maintain the potency and self-renewal of neurogenic ERGs during SC regeneration.

RESULTS

Tgf-β signaling is activated in dorsal ependymal progenitors after SCI.

Injuries to the central and peripheral nervous systems induce Tgf-β signaling across vertebrates. In mammals, Tgf-β activation directs a range of regenerative and anti-regenerative cell responses including immune cell activation, neurite outgrowth, and scar formation (Li et al., 2017). In zebrafish larvae, the anti-inflammatory effects of Tgfb1a are required for SC regeneration (Keatinge et al., 2021). We postulated that Tgf-β signaling is pro-regenerative in adult zebrafish. To explore this hypothesis, we first surveyed Smad3 phosphorylation as a readout of Tgf-β activity after zebrafish SCI. By immunohistochemistry, phosphorylated Smad3 (pSmad3) was strongly induced in dorsal SC tissues at 1 week post-injury (wpi) (Fig. 1A). pSmad3 expression gradually diminished between 2 and 3 wpi, and was minimally expressed in uninjured SCs (Fig. 1A). At 1 wpi, pSmad3^{+} cells accounted for 7% of dorsal SC cells, and were reduced by 3 wpi relative to 1 wpi (Fig 1B, S1A). To determine the identity of Tgf-β responsive cells after SCI, we co-labelled pSmad3 with either the neuronal markers HuC and HuD (HuC/D) or the ependymal progenitor marker Sox2. At 1 wpi, we rarely observed vesicular pSmad3 expression in some HuC/D^{+} neurons. However, the majority of HuC/D^{+} neurons were pSmad3^{-} (Fig. S1B). pSmad3 was primarily expressed at high levels in Sox2^{+} ERGs (Fig. 1C). Quantification revealed 66 to 76% of pSmad3^{+} cells were Sox2^{+} across timepoints (Fig. 1D, S1C). By EdU incorporation, ~10% of pSmad3^{+} cells were proliferative at 1 wpi in dorsal SCs, and pSmad3^{+} cell proliferation decreased to baseline levels by 3 wpi (Fig. S1D, E). These findings indicated Tgf-β signaling is activated in dorsal ERGs after SCI.

mstnb expression is upregulated in dorsal ependymal progenitors after SCI.

To explore mechanisms of Tgf-β activation during SC regeneration, we used a previously published RNA-seq dataset to survey the expression of Tgf-β ligands at 2 wpi (Mokalled et al., 2016). We found *mstnb*, *bmp2a/b*, and *bmp5* are upregulated, while *gdf3*, *gdf6a*, *gdf9*, *bmp6*, and *ndr1* are downregulated after injury relative to uninjured SC tissues (Fig. S1F). By fluorescence *in situ* hybridization, *mstnb* expression was induced in dorsal SC tissues between 1 and 2 wpi and decreased at 3 wpi (Fig. 1E-G). *mstnb* transcripts were not detectable in uninjured SCs (Fig. 1E-G). Co-labeling of *mstnb* transcripts with either ependymal Sox2 or neuronal HuC/D showed *mstnb* expression restricted to a subset of Sox2^{+} ERGs in dorsal SCs (Fig. 1F). *mstnb* transcripts

were excluded from neuronal cell bodies (Fig. 1G). These studies revealed *mstnb* expression is induced in a subset of dorsal ERGs after SCI, and suggested *mstnb* expression correlates with Tgf-β activation in dorsal SC tissues during SC regeneration.

mstnb is required for functional SC repair.

To examine the role of *mstnb* during SC regeneration, we analyzed the extent of functional and cellular recovery in genetic zebrafish mutants (*mstnb*^{bns5}) (Dogra et al., 2017) (Fig. 2A). *mstnb* mutants are adult viable, and elicit skeletal and cardiac muscle hyperplasia. Interestingly, the growth phenotypes associated with *mstnb* mutants are thought to be muscle specific (Dogra et al., 2017). To establish baseline motor function, we first assessed the swim capacities of wild-type, *mstnb* heterozygous (*mstnb*$^{+/-}$) and homozygous (*mstnb*$^{-/-}$) siblings in an enclosed swim tunnel under increasing water current velocities (Klatt Shaw and Mokalled, 2021; Klatt Shaw et al., 2021; Mokalled et al., 2016) (Fig. 2B). In this swim endurance assay, wild-type animals swam for 41 min before reaching exhaustion. *mstnb*$^{+/-}$ and *mstnb*$^{-/-}$ fish showed comparable swim functions, averaging 43 and 39 min of swim time, respectively. These results indicated *mstnb* mutants show normal swim capacity and suggested the muscle phenotype of *mstnb* mutants does not impact swim endurance. Next, we performed SC transections on *mstnb*$^{-/-}$ and control siblings and evaluated their functional regeneration between 2 and 6 wpi. *mstnb*$^{+/-}$ fish displayed normal swim capacity at 2 and 4 wpi, but their functional recovery was slightly compromised at 6 wpi (Fig. 2C). Relative to wild-type controls, functional recovery was 50% reduced in *mstnb*$^{-/-}$ fish at 2, 4, and 6 wpi (Fig. 2C).

To further rule out the contribution of skeletal muscle overgrowth to the functional regeneration output of *mstnb* mutants, we tracked the swim behavior of *mstnb* mutants in the absence of water current or under a constant, low current velocity of 10 cm/sec (Fig. 2D). We reasoned that, unlike the endurance test that required fish to swim against increasing current velocities, swim behavior under minimal current velocity is less likely to be dependent on muscle function. Fish position in the swim tunnel (Y position), percent activity, and burst frequency were quantified to assess overall swim competence. In this assay, *mstnb*$^{-/-}$ animals stalled in the back quadrant of the swim tunnel (Fig. 2E), were 65% less active than their wild-type siblings (Fig. 2F), and displayed less bursts under low current velocity (Fig. 2G). Consistent with a partial regeneration phenotype in heterozygous fish, *mstnb*$^{+/-}$ fish were 40% less active and their burst frequency was reduced by 35% relative to wild types at 2 wpi. Swim parameters were comparable between *mstnb*$^{+/-}$ and wild-type siblings at 4 and 6 wpi, and were not statistically significant at 2 wpi (Fig. 2E-G).

To date, cellular growth across the lesion site has served as a primary readout of cellular regeneration in zebrafish (Goldshmit et al., 2012; Mokalled et al., 2016; Reimer et al., 2013). Glial bridging and axon tracing assays were performed to evaluate the extents of glial and axonal regeneration across the lesion site (Fig. 2A). By Gfap immunostaining, glial bridging was unaffected in *mstnb*$^{-/-}$ animals compared to wild-type siblings at 2 wpi (Fig. 2H). At 4 wpi, anterograde axon tracing using Biocytin showed comparable axon regrowth in proximal and distal SC sections between *mstnb*$^{-/-}$ and control animals (Fig. 2I). Together, these studies indicated *mstnb* is required for functional SC repair but is dispensable for glial bridging and axonal regrowth across the lesion. These findings prompted us to investigate mechanisms of SC regeneration that are independent of glial bridging and axon growth.

mstnb is a negative regulator of adult neurogenesis after SCI

In addition to glial bridging and axon regrowth, zebrafish regenerate lost motor neurons and interneurons around the lesion site (Barreiro-Iglesias et al., 2015; Kuscha et al., 2012b; Reimer et al., 2008). Dorsal ependymal progenitors are thought to give rise to regenerating interneurons in dorsal SC tissues after injury. Since *mstnb* is expressed in dorsal ERGs after SCI and *mstnb* mutants did not show glial bridging or axon growth defects, we postulated that *mstnb* plays a role in adult neurogenesis in zebrafish and that local neurogenesis around the lesion is required for functional SC repair. To test this hypothesis, we first examined the proliferation rates of Sox2^{+} ERGs and of regenerating HuC/D^{+} neurons in *mstnb* mutants. Uninjured and injured *mstnb*$^{-/-}$ and wild-type siblings were subjected to SCI and to a single EdU pulse 24 hours prior to SC collection and histological analysis (Fig. 3A and S2A). Cell counts revealed a significant increase in HuC/D^{+} EdU^{+} neurons in dorsal SCs with 1 wpi SCs showing the most pronounced differences (Fig. 3B, C and S2B). At 1 wpi, 7.7% of HuC/D^{+} neurons were EdU^{+} in wild-type SCs (Fig. S2B), and accounted for 0.9% of dorsal SC cells (Fig. 3C). Conversely, 15.2% of HuC/D^{+} neurons were EdU^{+} in *mstnb*$^{-/-}$ SCs (Fig. S2B), accounting for 1.5% of dorsal SC cells (Fig. 3C). The rates of neurogenesis where attenuated in wild-type SCs at 2 and 3 wpi relative to 1 wpi. However, *mstnb* mutants showed increased neurogenesis at 3 wpi (Fig. 3C and S2B). These differences were blunted in cell counts from total SCs (Fig. S2C), suggesting neuronal differentiation is specifically increased in dorsal SC tissues of *mstnb* mutants. On the other hand, we observed a minor, non-significant decrease in the number of Sox2^{+} EdU^{+} ERGs in *mstnb*$^{-/-}$ SCs at 1 and 3 wpi (Fig. 3D, E and S2D, E). These findings indicated the rates of neurogenesis are increased in *mstnb* mutants.

To evaluate how snapshots of increased neurogenesis at 1 wpi could impact the numbers of regenerating neurons in *mstnb* mutants, we performed SC transections on *mstnb*$^{-/-}$ and wild-type fish followed by daily EdU injections for 1 or 2 wpi (Fig. 4A and S3A). In this assay, daily EdU labeling allowed us to estimate the total numbers of regenerating neurons (HuC/D^{+} EdU^{+} neurons), and the extent of self-renewal in ependymal progenitors (Sox2^{+} EdU^{+} ERGs). Considering the dynamic rates of neurogenesis along the rostro-caudal axis, we quantified cell numbers at 150, 450, and 750 μm rostral to the lesion. At 1 wpi and in wild-type sections proximal to the lesion site (-150 μm), 10.9% of dorsal SC cells were HuC/D^{+} neurons (Fig. 3C), and 2.7% of dorsal SC cells were regenerating neurons (HuC/D^{+} EdU^{+}) (Fig. 3D). On the other hand, 19% of dorsal SC cells were HuC/D^{+} neurons (Fig. 3C), and 4.3% of dorsal SC cells were regenerating neurons (HuC/D^{+} EdU^{+}) in *mstnb*$^{-/-}$ SCs (Fig. 3D). Quantifications from total SC tissues confirmed that the increase in regenerating neurons in *mstnb* mutants is specific to dorsal SCs and blunted in total SCs (Fig. S3B,C). At 2 wpi, the numbers of HuC/D^{+} EdU^{+} neurons continued to be elevated in *mstnb*$^{-/-}$ SCs (Fig. 4D). Intriguingly, the overall increase in the total numbers of neurons was less pronounced at this time point (Fig. 4C), suggesting *mstnb* mutants elicit an early wave of increased neurogenesis at 1 wpi, but that compensatory mechanisms may be activated at later time points to counteract the loss of *mstnb*. Finally, despite increased neurogenesis rates in *mstnb*$^{-/-}$ fish, the numbers of Sox2^{+} and Sox2^{+} EdU^{+} ERGs were comparable across genotypes (Fig. 4F,G), suggesting ERG self-renewal was maintained at normal levels in *mstnb* mutants. These studies revealed a 2-fold increase in regenerating neurons in *mstnb* mutants, and are consistent with *mstnb* acting as a negative regulator of adult neurogenesis in zebrafish.

Human MSTN proteins are translated as inactive full-length precursors that undergo proteolytic processing into mature MSTN peptide and MSTN proform (pro-MSTN) peptide. pro-MSTN exhibits high binding affinity for Myostatin and inhibits its function (Zhu et al., 2000). To examine whether the global effects of *mstnb* mutants could be reproduced by local Mstnb inhibition, we injured wild-type animals and performed daily injections of human recombinant MSTN Proform (pro-MSTN) peptide adjacent to the lesion site (Fig. S4A). We then assessed the numbers of HuC/D^{+} neurons and Sox2^{+} ERGs at 1 wpi, corresponding to 6 days after initial treatment. We found HuC/D^{+} neurons were increased by 12% upon pro-MSTN treatment, though these differences were not significant (Fig. S4B). On the other hand, the numbers of Sox2^{+} progenitors were decreased by 20% in pro-MSTN injected fish relative to vehicle controls (Fig. S4C). Consistent with genetic loss-of-function of *mstnb*, pharmacological Mstn inhibition at the

lesion site disrupted the relative ratios of HuC/D$^+$ neurons and Sox2$^+$ ERGs towards increased neurogenesis.

mstnb mutants exhibit increased neuronal differentiation after SCI

Our proliferation assays showed increased neurogenesis and suggested the rate of ERG self-renewal was slightly decreased in the absence of *mstnb*. To dissect the cellular basis for this phenotype, we evaluated the numbers of neural stem cells (NSCs) and intermediate neural progenitors (iNPs) in *mstnb* mutants at baseline, 1 and 2 wpi (Fig. 5A). We first combined a *nestin* reporter transgene (*nes:*GFP) with *mstnb*$^{-/-}$ background to quantify NSCs in *nes:*GFP;*mstnb*$^{-/-}$ fish (Lam et al., 2009) (Fig. 5B-D and S5A-C). *nes*:GFP$^+$ NSCs were rarely identified in uninjured SC sections from either mutant or wild-type animals, but were readily detectable after SCI (Fig. 5C and S5A). The proportions of *nes:*GFP$^+$ cells in dorsal or total SC tissues were comparable between *mstnb*$^{-/-}$ and wild-type siblings at either 1 or 2 wpi (Fig. 5C and S5A). At these time points, NSC proliferation showed decreasing trends in *mstnb* mutants (Fig. 5D), and was statistically significant when the numbers of *nes:*GFP$^+$ PCNA$^+$ cells were normalized to *nes:*GFP$^+$ NSCs (Fig. S5C). NSC proliferation was less pronounced in quantifications from total SC sections (Fig. S5B). These findings revealed NSC proliferation is reduced in *mstnb* mutants at 1 wpi.

The number of *nes*:GFP$^+$ NSCs were unaltered in *mstnb* mutants despite their decreased proliferation rate. We postulated that *mstnb* loss-of-function may bias NSC fate towards neuronal differentiation, and that compensatory mechanisms upstream of NSC activation maintain their total numbers across genotypes. To test this hypothesis, we examined the number of iNPs using *dbx1b:*GFP transgene bred into a *mstnb*$^{-/-}$ background (Pierani et al., 2001; Satou et al., 2012) (Fig. 5E-G and S5D,E). The proportion of *dbx1b:*GFP$^+$ iNPs averaged between 2.9 and 4.3 % of dorsal SC cells across time points, and showed an elevated trend in *mstnb*$^{-/-}$ relative to wild-type siblings at 2 wpi (Fig. 5F and S5D). These phenotypes were more pronounced in quantifications of *dbx1b:*GFP$^+$ PCNA$^+$ iNPs. Relative to wild-type siblings, *mstnb*$^{-/-}$ iNP proliferation was minimal prior to injury, increased by 2.3-fold at 1 wpi, and was normalized to wild-type levels by 2 wpi (Fig. 5G and S5E). These findings are consistent with accelerated neurogenesis in *mstnb* mutants.

To examine the differentiation and relative distribution of iNP-derived neurons after SCI, we labeled glycinergic neurons in *msntb* mutants using *slc6a5*:GFP reporter line (Fig. 5H-J and S5F) (McLean et al., 2007). At 1 wpi, the proportions of glycinergic neurons comprised 3.9% and 3.4%

of dorsal SC cells in *mstnb*$^{-/-}$ and wild-type fish, respectively (Fig. 5I and S5F). By 2 wpi, glycinergic neurons accounted for 1.2% of dorsal SC cells in wild-type controls, but increased to 2.7% of dorsal cells in *mstnb*$^{-/-}$ SCs (Fig. 5I and S5F). By quantifying the proportions of glycinergic neurons within HuC/D^{+} neurons, glycinergic neurons accounted for 6.1% and 3.7% of neurons in wild-type SC tissues at 1 and 2 wpi, respectively (Fig. 5J). These proportions were 2-fold elevated in *mstnb* mutants, accounting for 12% of neurons at 1 wpi and 8.5% of neurons at 2 wpi (Fig. 5J). Together, these results indicated *mstnb* mutants exhibit an expansion in glycinergic neurons, which are overrepresented relative to other neuronal cell populations.

Neuronal genes are upregulated in *mstnb* mutants

To determine the molecular mechanisms by which *mstnb* regulates the rates of neurogenesis, we deep sequenced SC tissues from *mstnb*$^{-/-}$ and wild-type siblings at 1 wpi, as well as uninjured controls (Fig. 6A-C). Principle component analysis confirmed clustering of biological replicates, and highlighted four distinct molecular signatures that are both injury- and genotype-induced (Fig. 6A). At 1 wpi, 61 genes were downregulated and 359 genes were upregulated in *mstnb*$^{-/-}$ SCs, suggesting *mstnb* may be a negative regulator of gene expression after SCI (Fig. 6C). Genes upregulated in *mstnb*$^{-/-}$ SCs comprised several neuronal or neuron differentiation genes, including *birc5b*, *eloal*, *elavl2*, *htr2aa*, and *pou5f3*, which were either unchanged or downregulated in uninjured *mstnb*$^{-/-}$ SCs (Fig. 6B-D). These findings indicated neuronal gene expression changes in *mstnb* mutants are injury-dependent.

Fibroblast growth factor (Fgf) maintains the proliferation and self-renewal capacities of neural stem cells in mammals (Hsu et al., 2009). By RNA-seq and qRT-PCR, *fgf1b* was downregulated in *mstnb*$^{-/-}$ SCs at 1wpi, but was unchanged in uninjured SC tissues (Fig. 6E). The dysregulation of *fgf1b* in *mstnb* mutants suggested *mstnb*-mediated *fgf1b* expression inhibits neurogenesis by promoting progenitor cell proliferation and self-renewal. To test this hypothesis, we examined whether the neuronal gene expression changes observed in *mstnb* mutants could be rescued by localized delivery of human recombinant FGF1 into SC lesions. We injured *mstnb*$^{-/-}$ and wild-type siblings and applied FGF1 proteins adjacent to the lesion site at 5 dpi using a gelfoam sponge. Gene expression changes were assessed by qRT-PCR at 1 wpi, corresponding to 2 days after treatment (Fig. 6F). Consistent with increased neurogenesis in *mstnb* mutants, *birc5b*, *eloal*, and *pou5f3* transcript levels were increased in vehicle-treated *mstnb*$^{-/-}$ relative to vehicle-treated wild-types (Fig. 6G). Application of exogenous FGF1 proteins at the lesion rescued the upregulation

of neuronal genes in *mstnb*$^{-/-}$ SCs (Fig. 6G). These findings indicated Mstn-mediated Fgf signaling is a negative regulator of adult neurogenesis after zebrafish SCI.

DISCUSSION

This study shows *mstnb* expression is induced in a subset of dorsal ERGs after SCI. Our results are consistent with a model in which *mstnb* regulates the rates of self-renewal and neuronal differentiation after SCI, and suggest *mstnb*-dependent Fgf signaling promotes self-renewal at the expense of neurogenesis (Fig. 6H).

Successful SC regeneration requires faithful recovery of the excitatory and inhibitory (E/I) balance in regenerating neural circuits. SCI alters the amount, strength, and relative locations of E/I inputs by disrupting descending hindbrain connections and promoting waves of axonal degeneration, neuronal death, and demyelination. Interneurons and motor neurons regenerate after zebrafish SCI. Notably, dopamine and serotonin signals from regenerating tracts control motor neuron regeneration by promoting the proliferation of pMN ERGs (Barreiro-Iglesias et al., 2015; Reimer et al., 2013). We found *mstnb* mutants display increased neuronal differentiation at 1 wpi, with an overrepresentation in glycinergic interneurons among regenerating neurons. Glycinergic inhibition plays important roles in coordinating locomotor rhythms in different organisms (Hinckley et al., 2005; Jovanović et al., 1999; Sibilla and Ballerini, 2009). We propose that increased inhibitory neurotransmission disrupts E/I balance and may underlie the behavioral recovery defects observed in *mstnb* mutants. The mechanisms that underlie E/I balance disruption in *mstnb* mutants require further investigation into the time course of neuronal regeneration and the contribution of *mstnb*$^{+}$ ERGs to specific neuronal populations.

Our study highlights a niche of dorsal ependymal progenitors that express *mstnb* after SCI. Unlike tissues that undergo constant cell renewal such as skin or blood, the nervous system undergoes little turnover and does not harbor a constitutively active neurogenic niche. Instead, neural progenitors are quiescent and are only activated upon physiological or pathological stimulation. Lineage restricted ependymal progenitors emerge after zebrafish SCI. ERG niches include a ventro-lateral domain that gives rise to regenerating motor neurons, and a ventral domain that undergoes epithelial-to-mesenchymal transition and is required for glial bridging after SCI (Klatt Shaw et al., 2021; Reimer et al., 2008). Our findings support the emergence of a lineage restricted, neurogenic niche of dorsal ERGs during SC regeneration in zebrafish. Consistent with this model, the numbers of motor neurons and the extent of glial bridging across the lesion, which

have been respectively associated with ventro-lateral and ventral ERGs, are unaffected in the absence of *mstnb*. Instead, *mstnb* mutants showed specific neurogenesis defects in dorsal SCs, and a preferential increase in dorsal glycinergic neurons. The molecular identity and cellular contributions of *mstnb*$^{+}$ ERGs to neurogenesis and SC repair warrant further investigation.

Niches of progenitor cells require intricate regulatory mechanisms to balance the rates of self-renewal, differentiation, and quiescence (Li and Clevers, 2010). At the cellular level, the organization of progenitor cells into localized niches maintains quiescence under homeostatic conditions, and triggers progenitor cell activation following niche disruption (Bagheri-Mohammadi, 2021). Molecularly, progenitor cell niches are hubs for Bmp, Wnt, and Notch signaling pathways, which control the rates of self-renewal, differentiation, and quiescence. Our study supports a model in which Mstn restricts neuronal differentiation and maintains neuronal progenitors in a proliferative, undifferentiated cell fate. Our findings are consistent with previously reported functions for Mstn in muscle, fat, and bone tissues (Dogra et al., 2017; Langley et al., 2002; Le and Yao, 2017; Lim et al., 2018; McCroskery et al., 2003; Wallner et al., 2017). Notably, previous findings have shown that Mstn is a regeneration limiting gene for zebrafish heart or fin regeneration, which are both dedifferentiation-based repair mechanisms (Dogra et al., 2017; Magga et al., 2019; Uribe et al., 2018). In contrast, in the context of SC regeneration, we find that Myostatin promotes regeneration by supporting regenerative FGF signaling, revealing a new role for Myostatin in this stem cell-based regeneration paradigm. Together these findings underline how tissue regeneration programs can coopt similar signaling pathways to achieve highly specific regenerative outcomes, and indicate a tissue-specific mechanism for Myostatin signaling.

We propose that Fgf is a mediator of Mstn functions during SC regeneration, and that Mstn limits neuronal differentiation by promoting Fgf-dependent self-renewal in *mstnb*$^{+}$ ERGs. Similar regulatory mechanisms have been shown in muscle tissues, where Mstn inhibits the muscle differentiation transcription factors MyoD and Myogenin. Fgf signaling promotes NSC proliferation and self-renewal (Hsu et al., 2009). In mammals, isolated ependymal cells have the capacity to form neurospheres and produce neurons, astrocytes and oligodendrocytes *in vitro* (Meletis et al., 2008). However, although mammalian SCI induces the proliferation of ependymal cells lining the central canal (Horner et al., 2000), mammalian ependymal cells are incapable of forming neurons *in vivo* (Barnabe-Heider et al., 2010; Muthusamy et al., 2018; Ren et al., 2017; Shah et al., 2018). We propose that comparative studies between zebrafish ERGs and mammalian ependymal cells

329 could reveal new insights into their differential regenerative capacities and examine whether Mstn
330 signaling is differentially regulated between zebrafish and mammals.

ACKNOWLEDGMENTS

We thank V. Cavalli, A. Johnson, K. Poss, and L. Solnica-Krezel for discussion, D. Stainier for sharing *mstnb* mutants, T. Li and B. Zhang for Bioinformatics analysis, and the Washington University Zebrafish Shared Resource for animal care. This research was supported by grants from the NIH (R01 NS113915 to M.H.M.) and the McDonnell Center for Cellular Neuroscience (to M.H.M.).

Figure 1

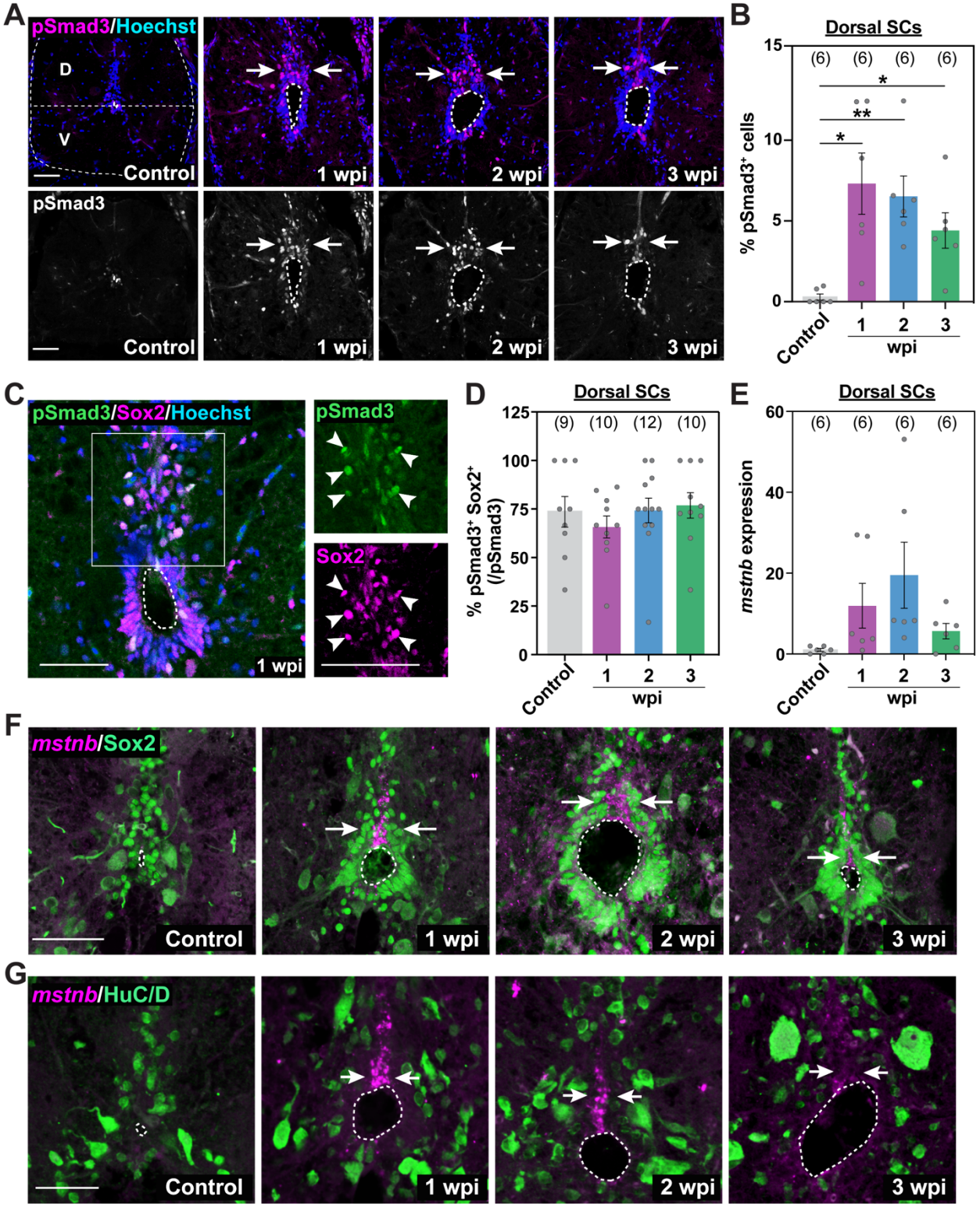

Figure 1. *mstnb* is induced in dorsal ependymal progenitors during SC regeneration. (A) Immunostaining for phosphorylated Smad3 (pSmad3) after SCI. Wild-type SC sections at 1, 2, and 3 wpi, and uninjured controls are shown. Cross sections 450μm from the lesion site are shown. Horizontal dotted line demarcates dorsal (D) and ventral (V) SC domains. Arrows point to $pSmad3^+$ nuclei in the dorsal domain. **(B)** pSmad3 quantification in dorsal sections of wild-type SCs. Percent $pSmad3^+$ cells was normalized to the number of nuclei in dorsal SCs. **(C)** pSmad3 and Sox2 immunostaining in wild-type SCs at 1 wpi. High-magnification views of dorsal SCs are shown. Arrowheads point to $pSmad3^+$ $Sox2^+$ ERGs. **(D)** pSmad3 quantification in dorsal ERGs. Percent $pSmad3^+$ $Sox2^+$ cells was normalized to the number of $pSmad3^+$ cells. **(E)** Quantification of *mstnb* by *in situ* hybridization in dorsal SC tissues. **(F,G)** *mstnb* expression in wild-type SC sections after SCI. *mstnb* fluorescence *in situ* hybridization was followed by immunostaining for either Sox2 (F) or HuC/D (G) antibodies. Cross sections 450μm from the lesion site are shown at 1 , 2, and 3 wpi, and for uninjured controls. Arrows point to domains of *mstnb* expression in dorsal SCs. Dotted ovals delineate central canal edges. For all quantification, SC sections 450 μm rostral to the lesion were analyzed and sample sizes are indicated in parentheses. *P<0.05; **P<0.01. Scale bars, 50 μm.

Figure 2

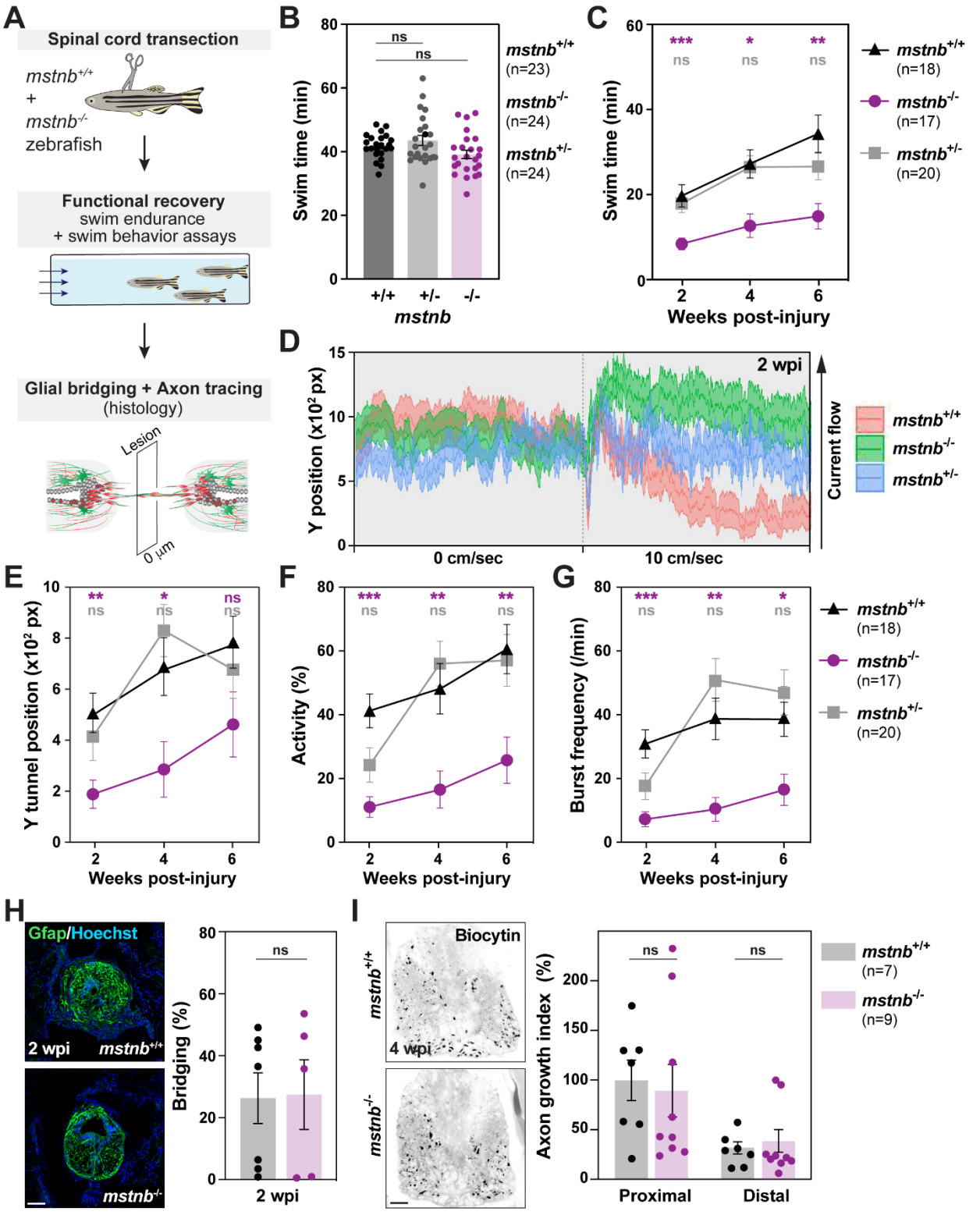

Figure 2. *mstnb* is required for functional SC regeneration. (A) Experimental pipeline to examine regeneration phenotypes after SCI. *mstnb*$^{-/-}$ fish and wild-type siblings were subjected to complete SC transection. Functional recovery was assessed between 2 and 6 wpi. Histology was used to assess glial and axonal bridging at 2 and 4 wpi, respectively. **(B)** Endurance swim assays determined baseline motor function for *mstnb*$^{-/+}$, *mstnb*$^{-/-}$, and wild-type fish. Dots represent individual animals from three independent clutches. **(C)** Endurance swim assays for *mstnb*$^{-/+}$, *mstnb*$^{-/-}$, and wild-type fish at 2, 4, and 6 wpi. Dots represent individual animals from two independent experiments. Statistical analyses of swim times are shown for *mstnb*$^{-/+}$ (grey) and *mstnb*$^{-/-}$ (magenta) relative to wild types. Recovery of *mstnb*$^{-/-}$ animals was not significant between 2 and 6 wpi. **(D)** Tracking swim performance at minimal water current velocity for *mstnb*$^{-/+}$ (blue), *mstnb*$^{-/-}$ (green), and wild-type siblings (red). Average Y position is shown for each cohort at 2 wpi. Animals were tracked in the absence of current (0 cm/sec) for 5 min, and for a 10cm/sec current velocity for 5 min. The arrow shows the direction of the water current. **(E-G)** Average Y position in the tunnel (E), percent activity (F), and burst frequency (G) were quantified at 10 cm/sec water current velocity. *mstnb*$^{-/+}$, *mstnb*$^{-/-}$, and wild-type fish are shown at 2, 4, and 6 wpi. Statistical analyses of swim times are shown for *mstnb*$^{-/+}$ (grey) and *mstnb*$^{-/-}$ (magenta) relative to wild types. Two independent experiments are shown. **(H)** Glial bridging in *mstnb*$^{-/-}$ (magenta) and wild-type siblings (grey) at 2 wpi. Representative immunohistochemistry shows the Gfap^{+} bridge at the lesion site. Percent bridging represents the cross-sectional area of the glial bridge at the lesion site relative to the the intact SC. Percent bridging was quantified for 7-9 animals per group. **(I)** Anterograde axon tracing in in *mstnb*$^{-/-}$ (magenta) and wild-type zebrafish (grey) at 4 wpi. Biocytin axon tracer was applied rostrally and analyzed at 100 μm (proximal) and 500 μm (distal) caudal to the lesion. Representative traces of biocytin are shown for each genotype animals at the proximal level. Quantification represents 7-9 animals per group. Axon growth was normalized to Biocytin labeling in wild-types at the proximal level. *P<0.05; **P<0.01; ***p<0.001; ns, not significant. Scale bars, 50 μm.

Figure 3

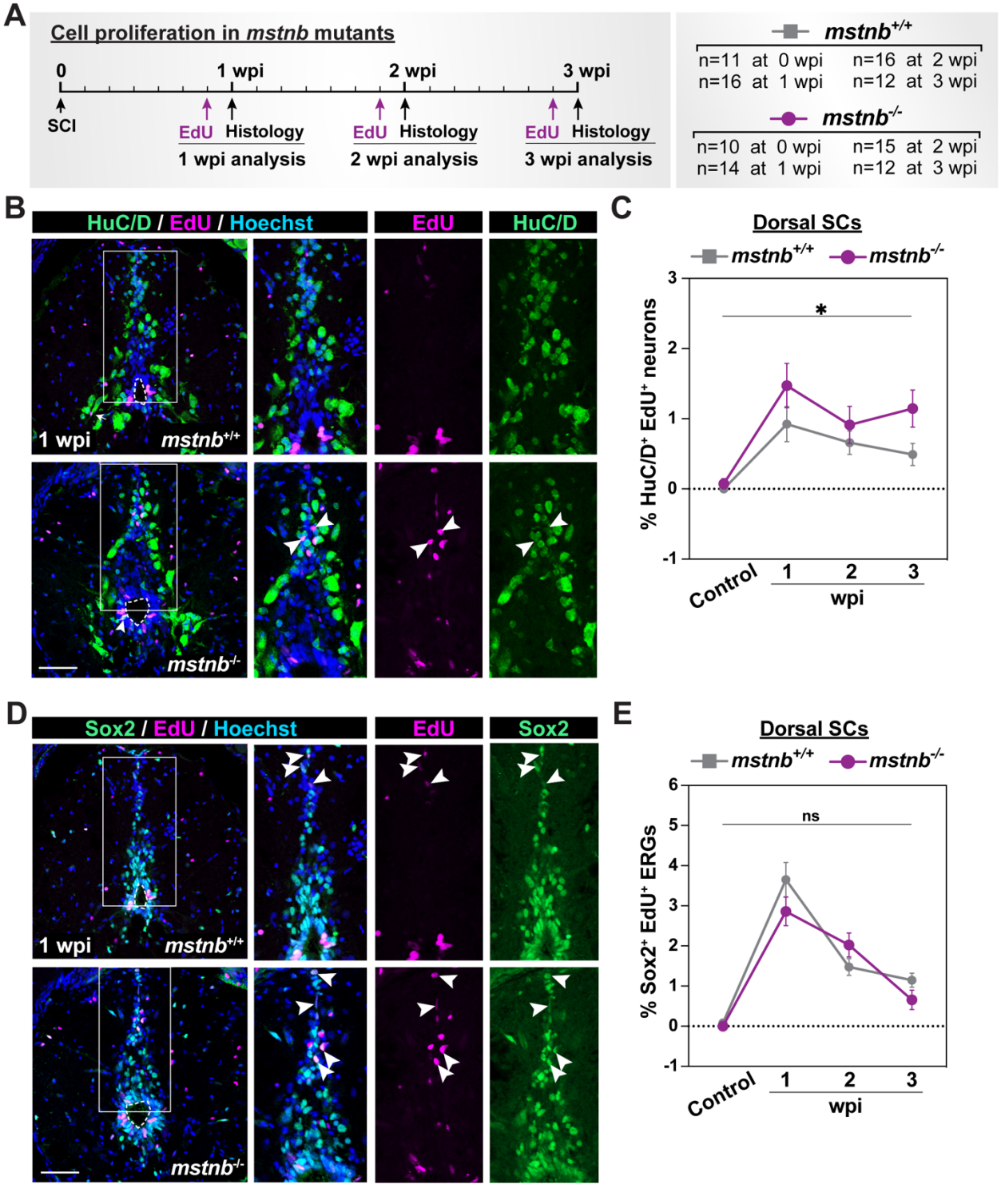

Figure 3. Cell proliferation in *mstnb* mutant zebrafish. (A) Experimental timeline to assess the rates of cell proliferation. *mstnb*$^{-/-}$ and wild-type siblings were subjected to SC transections. A single EdU injection was performed at either 6, 13, or 20 days post-injury. SC tissues were harvested for analysis at 1, 2, 3 wpi and at 24 hours after EdU injection. Animal numbers are indicated for each genotypes and two independent replicates are shown. **(B)** Immunohistochemistry for EdU and HuC/D in SC sections of *mstnb*$^{+/+}$ and *mstnb*$^{-/-}$ at 1 wpi. The region inside the rectangular box is shown in higher magnification. Arrowheads indicate HuC/D^{+} EdU^{+} neurons. **(C)** Regenerated HuC/D^{+} EdU^{+} neurons were quantified in dorsal SC sections at 1, 2, 3 wpi and uninjured controls. Percent HuC/D^{+} EdU^{+} neurons was normalized to the total number of nuclei for each section. **(D)** Immunohistochemistry for EdU and Sox2 in SC sections of *mstnb*$^{+/+}$ and *mstnb*$^{-/-}$ at 1 wpi. The region inside the rectangular box is shown in higher magnification. Arrowheads indicate Sox2^{+} EdU^{+} ERGs. **(E)** Sox2^{+} EdU^{+} ERGs were quantified in dorsal SC sections at 1, 2, 3 wpi and uninjured controls. Percent Sox2^{+} EdU^{+} ERGs was normalized to the total number of nuclei for each section. For all quantifications, cross SC sections 450 μm rostral to the lesion site were quantified.*P<0.05; ns, not significant. Scale bars, 50 μm. Dotted ovals delineate central canal edges.

Figure 4

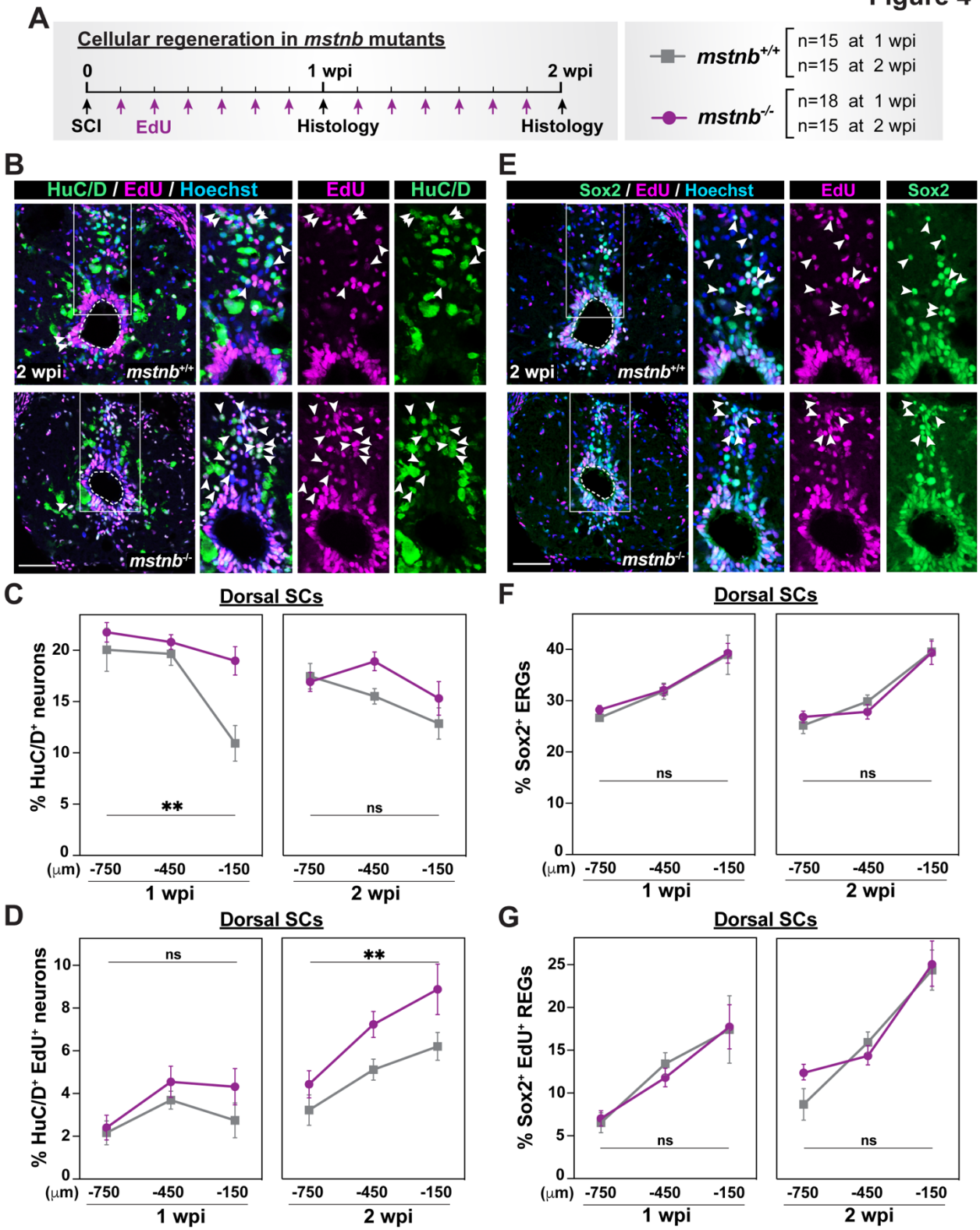

Figure 4. Regenerative neurogenesis in *mstnb* mutant zebrafish. (A) Experimental timeline to assess the rates of neurogenesis and ERG self-renewal. *mstnb*$^{-/-}$ and wild-type siblings were subjected to SC transections and daily EdU injections. SC tissues were harvested for analysis at 1 or 2 wpi. Animal numbers are indicated for each genotypes and two independent replicates are shown. **(B)** Immunohistochemistry for EdU and HuC/D in SC sections of *mstnb*$^{+/+}$ and *mstnb*$^{-/-}$ at 2 wpi. The region inside the rectangular box is shown in higher magnification. Arrowheads indicate HuC/D^{+} EdU^{+} neurons. **(C)** HuC/D^{+} neurons were quantified in dorsal SC sections at 1 and 2 wpi. Percent HuC/D^{+} neurons was normalized to the total number of nuclei for each section. **(D)** Regenerated HuC/D^{+} EdU^{+} neurons were quantified in dorsal SC sections at 1 and 2 wpi. Percent HuC/D^{+} EdU^{+} neurons was normalized to the total number of nuclei for each section. **(E)** Immunohistochemistry for EdU and Sox2 in SC sections of *mstnb*$^{+/+}$ and *mstnb*$^{-/-}$ at 2 wpi. The region inside the rectangular box is shown in higher magnification. Arrowheads indicate Sox2^{+} EdU^{+} ERGs. **(F)** Sox2^{+} ERGs were quantified in dorsal SC sections at 1 and 2 wpi. Percent Sox2^{+} ERGs was normalized to the total number of nuclei for each section. **(G)** Sox2^{+} EdU^{+} ERGs were quantified in dorsal SC sections at 1 and 2 w. Percent Sox2^{+} EdU^{+} ERGs was normalized to the total number of nuclei for each section. For all quantifications, cross SC sections at 150, 450, and 750 μm rostral to the lesion site were quantified. **P<0.01; ns, not significant. Scale bars, 50 μm. Dotted lines delineate central canal edges.

Figure 5

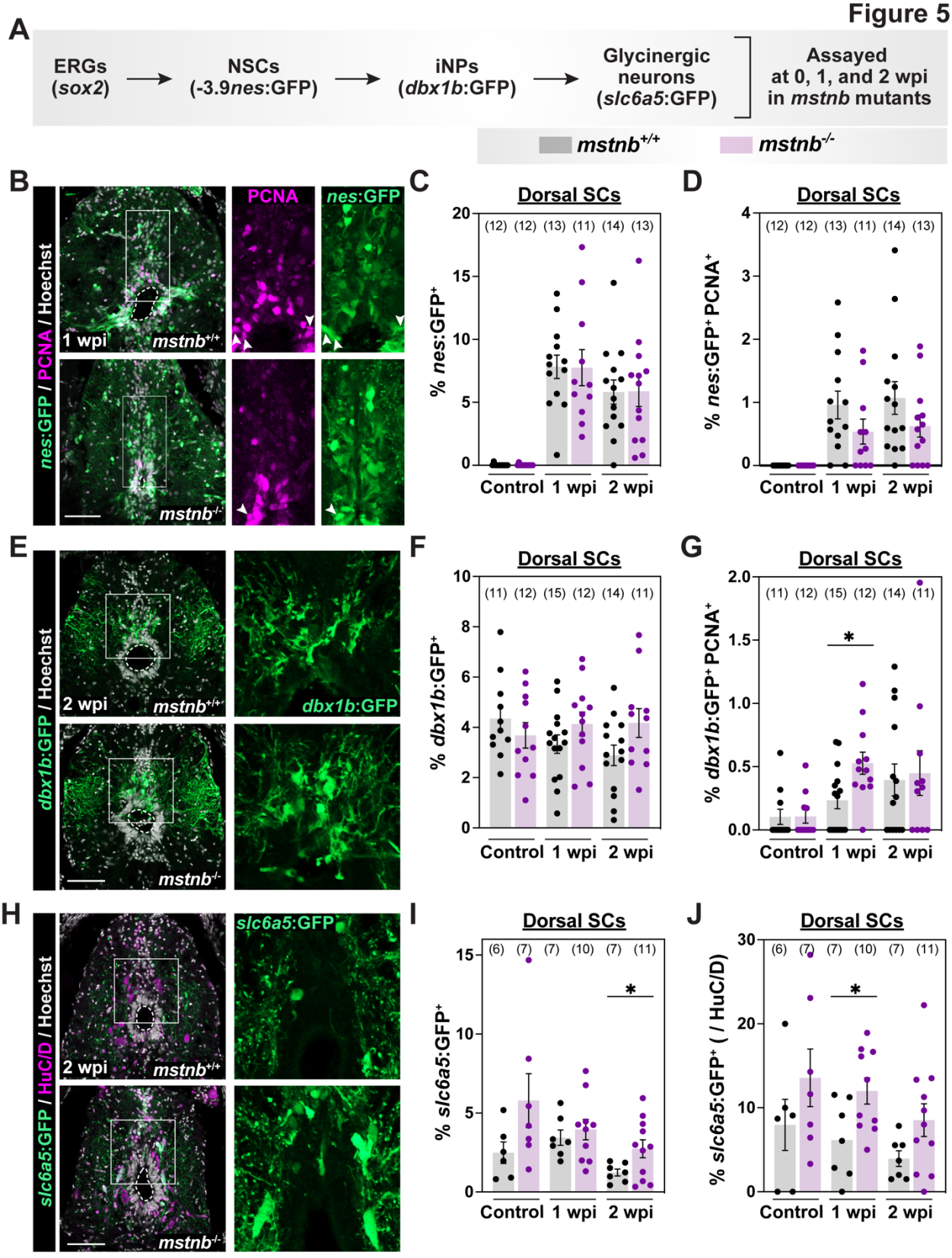

Figure 5. Assessment of neuronal progenitors and neurons in *mstnb* mutant zebrafish. **(A)** Experimental timeline to elucidate the dynamics of neurogenesis. *mstnb*$^{-/-}$ animals were crossed into either -*3.9nestin*:GFP, *dbx1b*:GFP, or *slc6a5*:GFP to evaluate the numbers of neural stem cells (NSCs), intermediate neural progenitors (iNPs), and glycinergic neurons, respectively. *mstnb*$^{-/-}$ and wild-type siblings were subjected to SC transections and collected at 1 or 2 wpi for analysis. Uninjured controls were used. Animal numbers are indicated for each genotypes and two independent replicates are shown. **(B)** GFP and PCNA staining in -*3.9nestin*:GFP*;mstnb*$^{-/-}$ SC sections at 1 wpi. -*3.9nestin*:GFP*;mstnb*$^{+/+}$ siblings are used as controls. The region inside the rectangular box is shown in higher magnification. **(C)** *nes*$^{+}$ NSCs were quantified in dorsal SC sections. Percent *nes*$^{+}$ NSCs was normalized to the total number of nuclei for each section. **(D)** *nes*$^{+}$ PCNA^{+} NSCs were quantified in dorsal SC sections. Percent *nes*$^{+}$ PCNA^{+} NSCs was normalized to the total number of nuclei for each section. **(E)** GFP staining in *dbx1b*:GFP*;mstnb*$^{-/-}$ SC sections at 2 wpi. *dbx1b*:GFP*;mstnb*$^{+/+}$ siblings are used as controls. The region inside the rectangular box is shown in higher magnification. **(F)** *dbx1b*$^{+}$ iNPs were quantified in dorsal SC sections. Percent *dbx1b*$^{+}$ iNPs was normalized to the total number of nuclei for each section. **(G)** *dbx1b*$^{+}$ PCNA^{+} NSCs were quantified in dorsal SC sections. Percent *dbx1b*$^{+}$ PCNA^{+} iNPs was normalized to the total number of nuclei for each section. **(H)** GFP staining in *slc6a5*:GFP:GFP*;mstnb*$^{-/-}$ SC sections at 2 wpi. *slc6a5*:GFP:GFP*;mstnb*$^{+/+}$ siblings are used as controls. The region inside the rectangular box is shown in higher magnification. **(I)** *slc6a5*:GFP^{+} glycinergic neurons were quantified in dorsal SC sections. Percent *slc6a5*:GFP^{+} neurons was normalized to the total number of nuclei for each section. **(J)** Percent *slc6a5*:GFP^{+} neurons was normalized to the numbers of HuC/D^{+} neurons for each section. Dotted ovals delineate central canal edges. For all quantifications, cross SC sections 450 μm rostral to the lesion site were quantified. *P<0.05; ns, not significant. Scale bars, 50 μm.

Figure 6

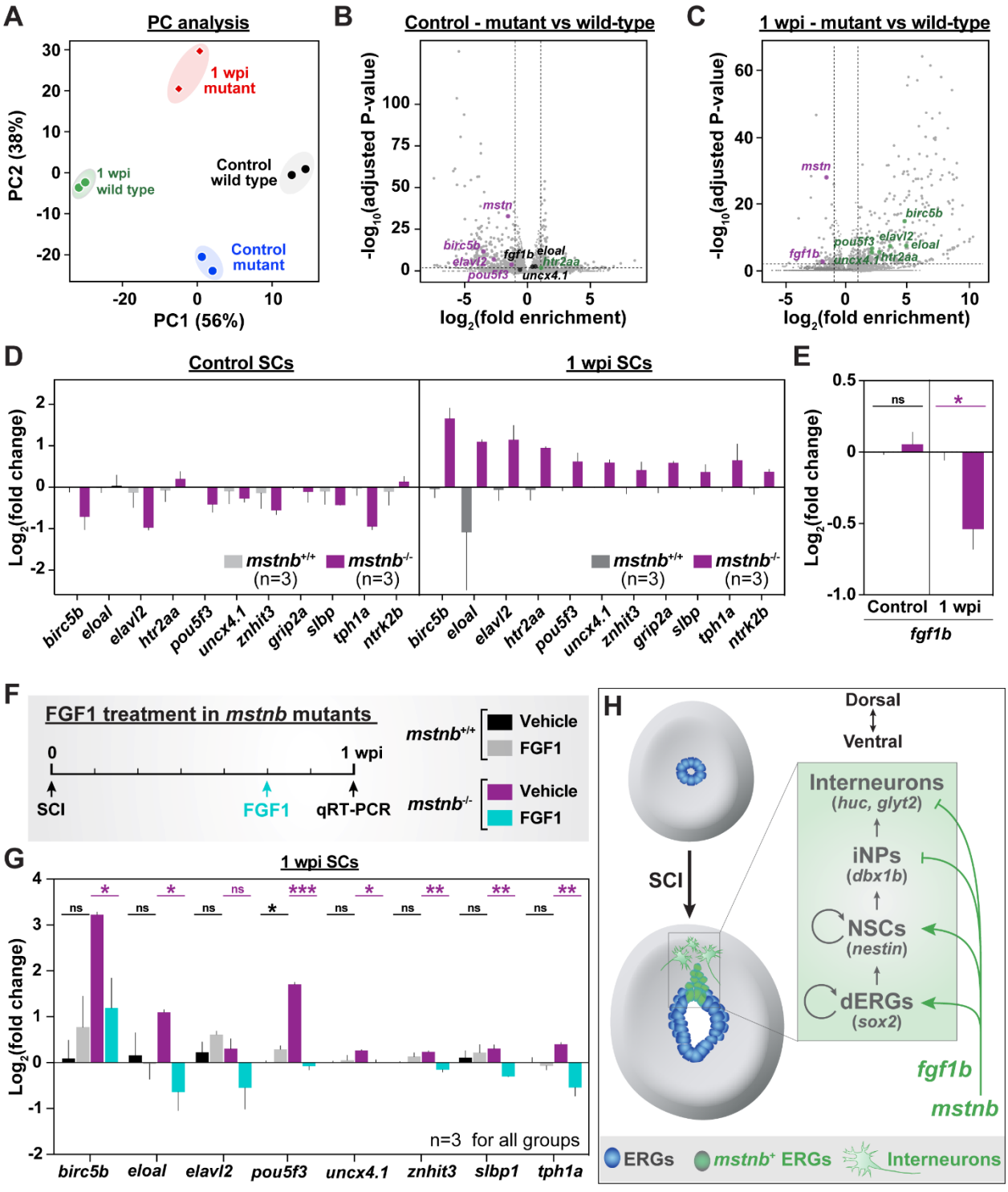

Figure 6. *mstnb* regulates neuronal gene expression via *fgf1b*. (A) *mstnb*$^{-/-}$ and wild-type siblings were subjected to complete SC transections and collected at 1 wpi for RNA sequencing. Control SC tissues were collected from uninjured fish. Sequencing was performed in independent duplicates. Principle component analysis shows clustering of biological replicates. Principle components 1 and 2 (PC1 and PC 2) show 56% and 38% variance, respectively. **(B,C)** Volcano plot representation of genes that are significantly upregulated or downregulated or depleted in *mstnb*$^{-/-}$ SCs relative to wild-type controls. Upregulated genes included genes with $\log_2$ (fold enrichment) > 1 and adjusted P-value <0.01. Downregulated genes included genes with $\log_2$ (fold enrichment) < -1 and adjusted P-value <0.01 are considered downregulated. Select upregulated (green) and downregulated (magenta) neuronal genes are indicated. Unchanged genes are labelled in black. **(D)** qRT-PCR for neuronal genes was performed on *mstnb*$^{-/-}$ and wild-type SCs at 1 wpi. Uninjured *mstnb*$^{-/-}$ and wild-type controls were used. For each time point, $\log_2$ (fold change) was normalized to *eif1α* and to gene expression levels in *mstnb*$^{+/+}$ controls. **(E)** *fgf1b* qRT-PCR was performed on uninjured and injured *mstnb*$^{-/-}$ and wild-type animals. For each time point, *fgf1b* expression was normalized to *eif1α* as a loading control and to *fgf1b* levels in *mstnb*$^{+/+}$ controls. **(F)** *mstnb*$^{-/-}$ and wild-type siblings were subjected to SC transections and treated with gelfoam-soaked human recombinant FGF1 at 5 dpi. *mstnb*$^{-/-}$ and wild-type controls were treated with vehicle-soaked gelfoam. SCs were collected for gene expression analysis at 1 wpi, which corresponds to 2 days post-treatment. Animal numbers are indicated for each genotype. **(G)** Neuronal gene expression was analyzed by qRT-PCR from FGF1- and vehicle-treated SC tissues. For each gene, $\log_2$ (fold change) was normalized to *eif1α* as a loading control and to gene expression levels in uninjured *mstnb*$^{+/+}$ SCs. **(H)** Schematic model shows *mstnb* is a negative regulator of neuronal differentiation in dorsal SC tissues after spinal cord injury. ERGs (blue) undergo extensive proliferation after SCI. A *mstnb* expressing niche (green) emerges in the dorsal ependyma.

Figure S1

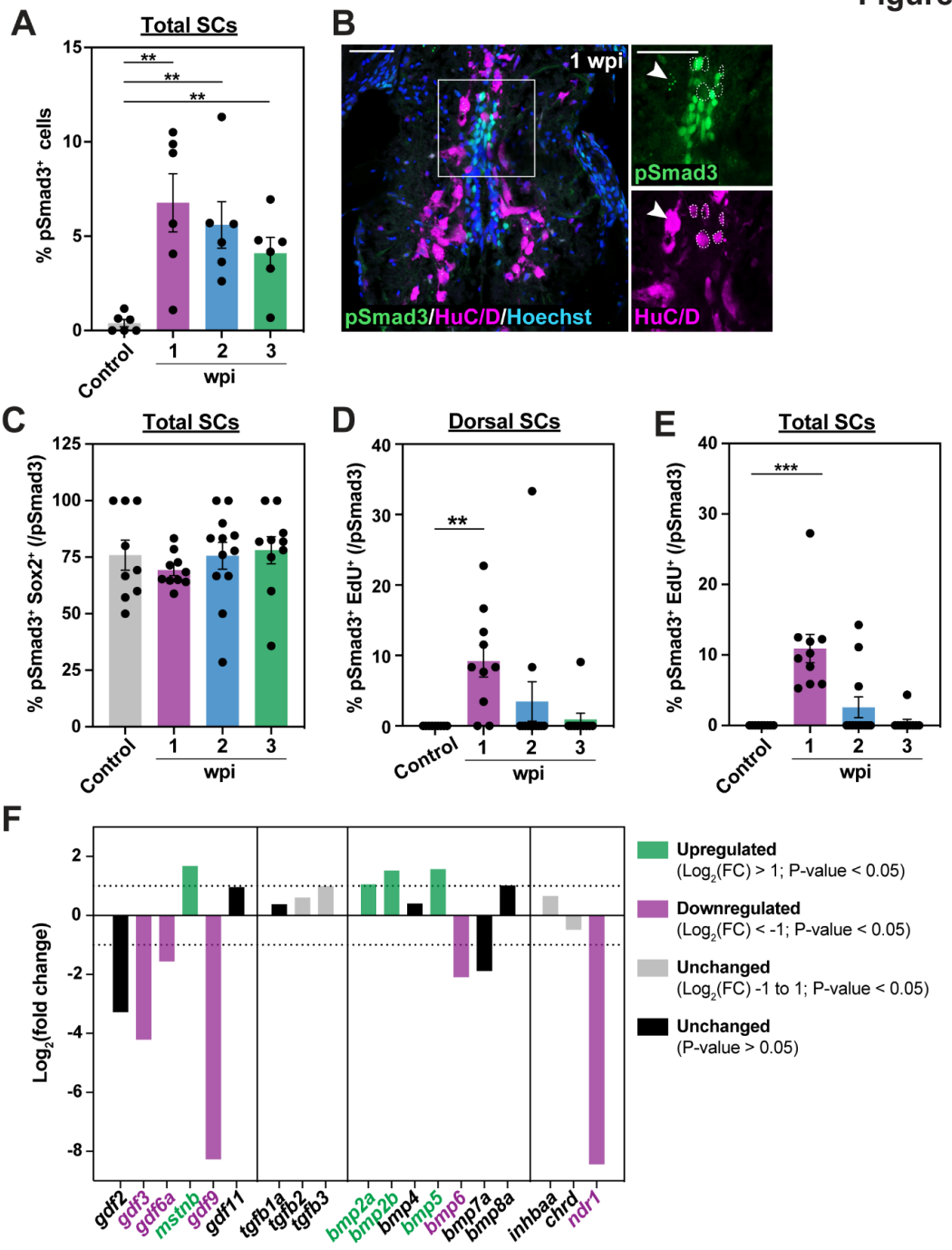

Figure S1. TGF-β signaling during SC regeneration. **(A)** pSmad3 quantification in total SC sections. Wild-type SCs at 1, 2 and 3 wpi and uninjured SCS were analyzed. Percent $pSmad3^+$ cells was normalized to the number of nuclei in dorsal SCs. **(B)** pSmad3 and HuC/D immunostaining in wild-type SCs at 1 wpi. High-magnification views of dorsal SCs are shown. Dotted lines delineate $pSmad3^-$ HuC/D^+ neurons. Arrowheads point to dotted pSmad3 expression in a subset of HuC/D^+ neurons. **(C)** pSmad3 quantification in total ERGs. Wild-type SCs at 1, 2 and 3 wpi and uninjured SCS were analyzed. Percent $pSmad3^+$ $Sox2^+$ cells was normalized to the number of $pSmad3^+$ cells. **(D, E)** pSmad3 and EdU quantification in dorsal (D) and total (E) SCs. EdU was administered for 24 hrs prior to SC collection. Wild-type SCs at 1, 2 and 3 wpi and uninjured SCS were analyzed. Percent $pSmad3^+$ EdU^+ cells was normalized to the number of $pSmad3^+$ cells. **(F)** Expression of Tgf-β ligands in wild-type SCs at 2 wpi by bulk RNA sequencing. For each gene, $\log_2$ (fold change) was normalized to gene expression levels in sham injured SCs. Upregulated (green) and downregulated (magenta) genes are shown. Unchanged genes are shown in grey and black. For all quantifications, cross SC sections 450 μm rostral to the lesion site were quantified. ***P<0.001; **P<0.01. Scale bars, 50 μm.

Figure S2

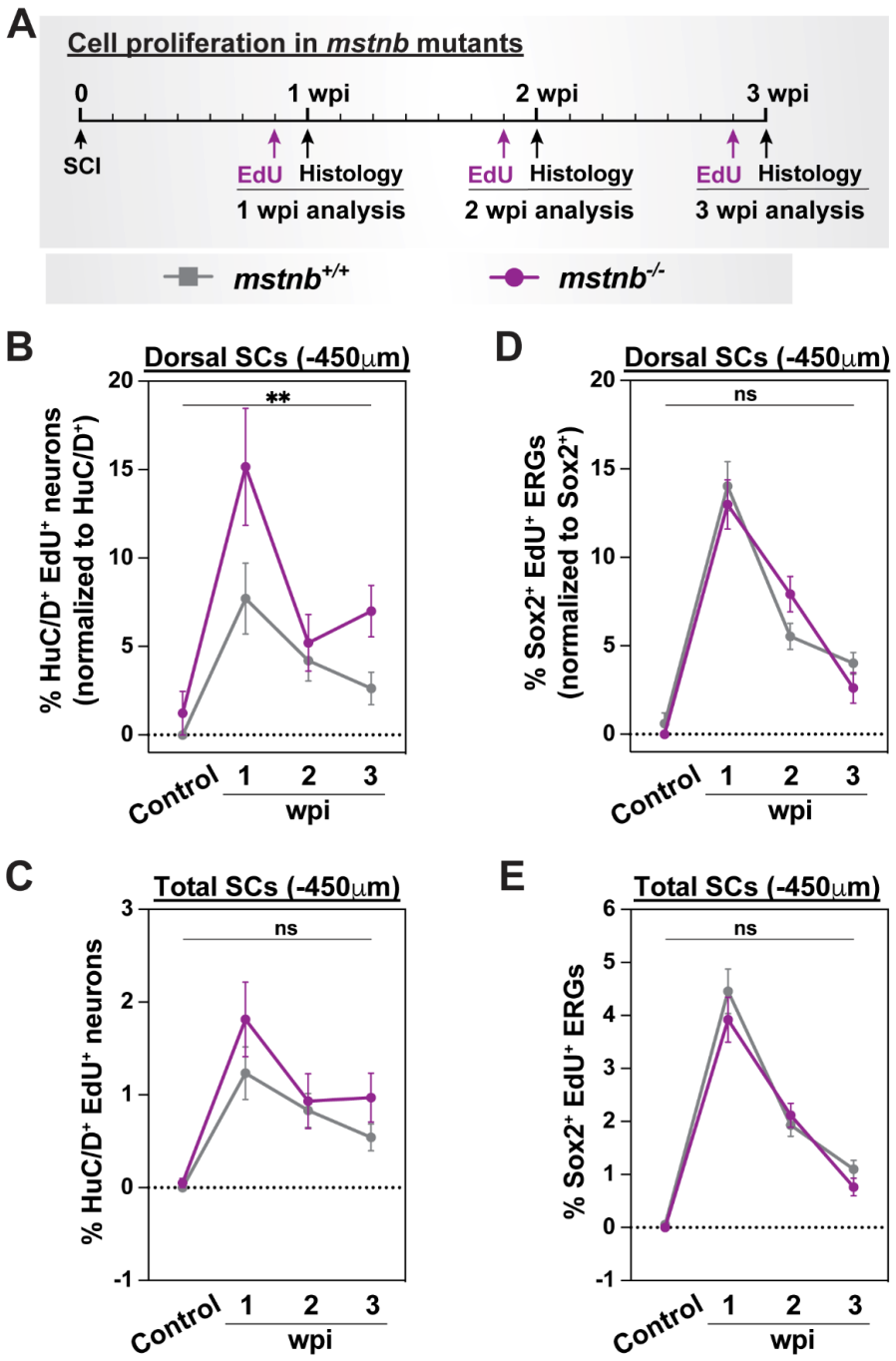

Figure S2. Cell proliferation in *mstnb* mutant zebrafish. (A) Experimental timeline to assess the rates of cell proliferation. *mstnb*$^{-/-}$ and wild-type siblings were subjected to SC transections. A single EdU injection was performed at either 6, 13, or 20 days post-injury. SC tissues were harvested for analysis at 1, 2, 3 wpi and at 24 hours after EdU injection. Animal numbers are indicated for each genotypes and two independent replicates are shown. **(B)** Regenerated HuC/D^{+} EdU^{+} neurons were quantified in dorsal SC sections at 1, 2, 3 wpi and uninjured controls. Percent HuC/D^{+} EdU^{+} neurons was normalized to the total number of HuC/D^{+} neurons for each section. **(C)** Regenerated HuC/D^{+} EdU^{+} neurons were quantified in total SC sections at 1, 2, 3 wpi and uninjured controls. Percent HuC/D^{+} EdU^{+} neurons was normalized to the total number of nuclei for each section. **(D)** Sox2^{+} EdU^{+} ERGs were quantified in dorsal SC sections at 1, 2, 3 wpi and uninjured controls. Percent Sox2^{+} EdU^{+} ERGs was normalized to the total number of Sox2^{+} ERGs for each section. **(E)** Sox2^{+} EdU^{+} ERGs were quantified in total SC sections at 1, 2, 3 wpi and uninjured controls. Percent Sox2^{+} EdU^{+} ERGs was normalized to the total number of nuclei for each section. For all quantifications, cross SC sections 450 μm rostral to the lesion site were quantified.**P<0.01; ns, not significant.

Figure S3

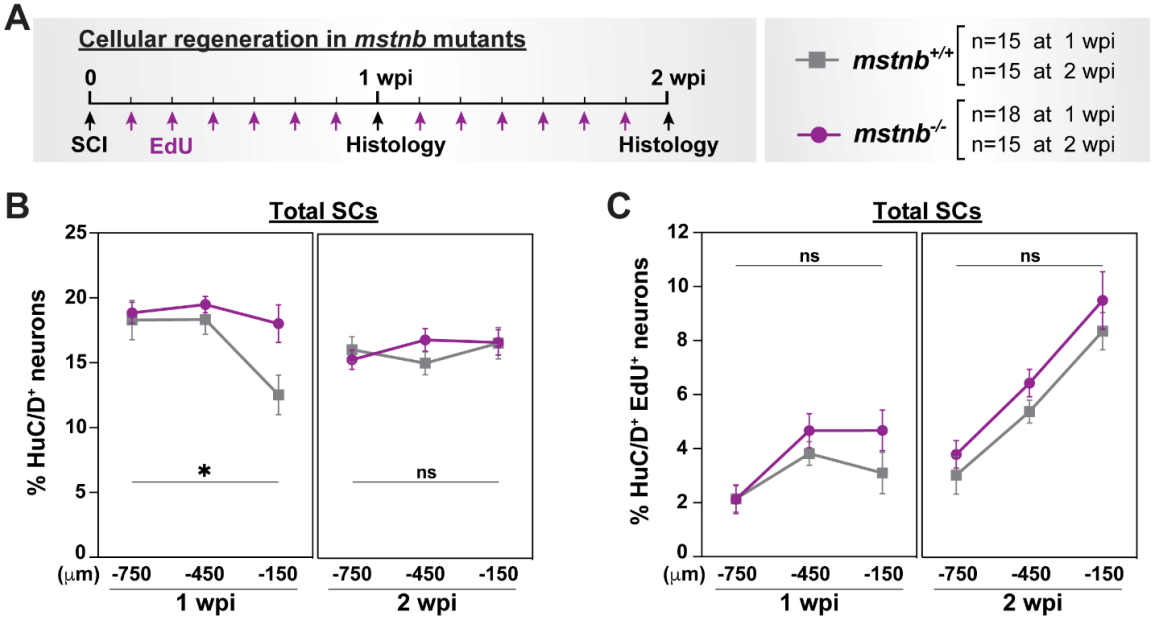

Figure S3. Regenerative neurogenesis in *mstnb* mutant zebrafish. (A) Experimental timeline to assess the rates of neurogenesis and ERG self-renewal. *mstnb*$^{-/-}$ and wild-type siblings were subjected to SC transections and daily EdU injections. SC tissues were harvested for analysis at 1 or 2 wpi. Animal numbers are indicated for each genotypes and two independent replicates are shown. **(C)** HuC/D^{+} neurons were quantified in total SC sections at 1 and 2 wpi. Percent HuC/D^{+} neurons was normalized to the total number of nuclei for each section. **(D)** Regenerated HuC/D^{+} EdU^{+} neurons were quantified in total SC sections at 1 and 2 wpi. Percent HuC/D^{+} EdU^{+} neurons was normalized to the total number of nuclei for each section. For all quantifications, cross SC sections at 150, 450, and 750 μm rostral to the lesion site were quantified. **P<0.01; ns, not significant.

Figure S4

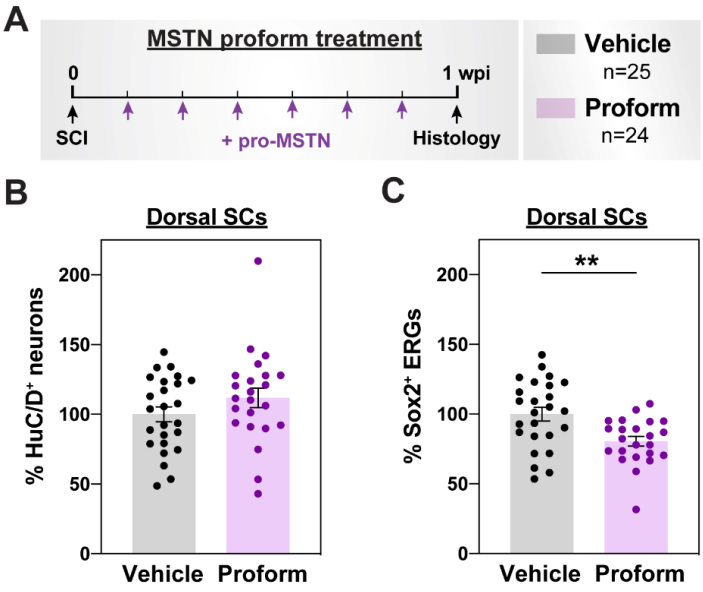

Figure S4. Pharmacological Mstn inhibition during SC regeneration. (A) For local Mstnb inhibition, wild-type SCs were subjected to SC transections and daily injections of human recombinant MSTN Proform (pro-MSTN) peptide adjacent to the lesion site. SC tissues were harvested for analysis at 1 wpi. Animal numbers are indicated for each genotypes and two independent replicates are shown. **(B)** HuC/D^{+} neurons were quantified in pro-MSTN- and vehicle-treated SCs. Dorsal SC sections at 1 wpi were analyzed. Percent HuC/D^{+} neurons was normalized to the total number of nuclei for each section. **(C)** Sox2^{+} ERGs were quantified in pro-MSTN- and vehicle-treated SCs. Dorsal SC sections at 1 wpi were analyzed. Percent Sox2^{+} ERGs was normalized to the total number of nuclei for each section. For all quantifications, cross SC sections 450 μm rostral to the lesion site were quantified. **P<0.01.

Figure S5

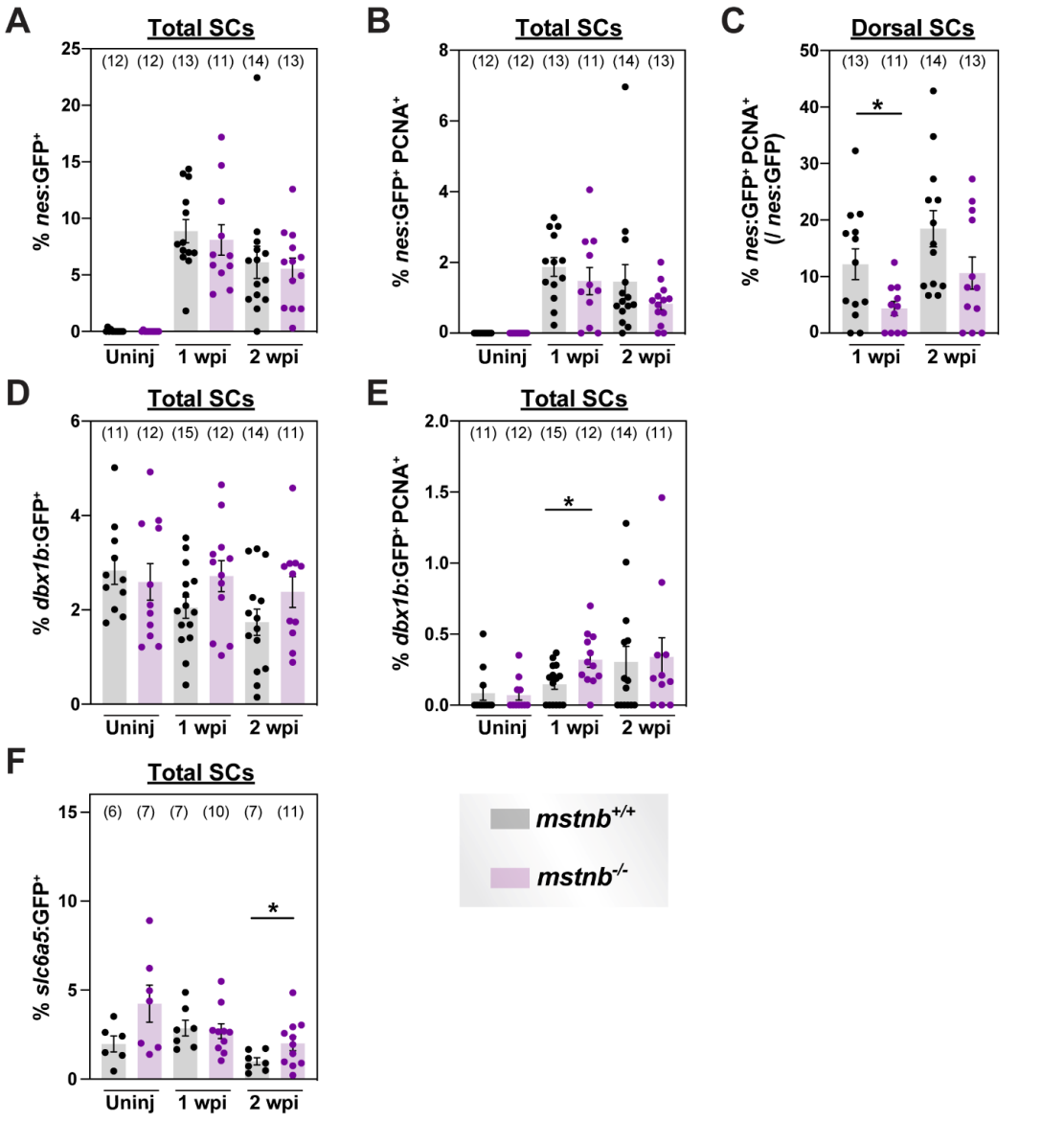

Figure S5. Assessment of neuronal progenitors and neurons in *mstnb* mutant zebrafish. **(A)** *nes*$^{+}$ NSCs were quantified in total SC sections. Percent *nes*$^{+}$ NSCs was normalized to the total number of nuclei for each section. **(B)** *nes*$^{+}$ PCNA^{+} NSCs were quantified in total SC sections. Percent *nes*$^{+}$ PCNA^{+} NSCs was normalized to the total number of nuclei for each section. **(C)** *nes*$^{+}$ PCNA^{+} NSCs were quantified in dorsal SC sections. Percent *nes*$^{+}$ PCNA^{+} NSCs was normalized to the total number of *nes*$^{+}$ NSCs for each section. **(D)** *dbx1b*$^{+}$ iNPs were quantified in total SC sections. Percent *dbx1b*$^{+}$ iNPs was normalized to the total number of nuclei for each section. **(E)** *dbx1b*$^{+}$ PCNA^{+} iNPs were quantified in total SC sections. Percent *dbx1b*$^{+}$ PCNA^{+} NSCs was normalized to the total number of nuclei for each section. **(F)** *slc6a5*:GFP^{+} glycinergic neurons were quantified in total SC sections. Percent *slc6a5*:GFP^{+} neurons was normalized to the total number of nuclei for each section. For all quantifications, cross SC sections 450 μm rostral to the lesion site were quantified. *P<0.05.

Gene	Primer Name	Sequence	Product size
birc5b	bric5b_exon1_fwd	CGAGAAGATTGCCAGTGCACAC	70
	bric5b_exon2_rev	CATTCTCACTGGGACAGTGAAC	
eloal	eloal_exon1_fwd	GCTGAAGGAATGTAATGATG	74
	eloal_exon2_rev	CAAGTGTGATGTCCAATACTTC	
elavl2	elavl2_exon3_fwd	GAGATCGAGTCCTGCAAACTCG	79
	elavl2_exon4_rev	GCTCCATATAGTTCACAAAGCCG	
htr2aa	htr2aa_exon1_fwd	GTCATGCCAGTCTCCATGGTG	74
	htr2aa_exon2_rev	CACATGGGACACAGTGATGC	
pou5f3	pou5f3_exon3_fwd	GAACGAGGCCGAAAACTCCGAG	67
	pou5f3_exon4_rev	CGTGTCGACAAACACCCGTTC	
uncx4.1	uncx4.1_exon2_fwd	GCTACGTCTAGACCTTGTTGAG	65
	uncx4.1_exon3_rev	GCCATTTGGCTCGCCGGTTTTG	
znhit3	znhit3_exon3_fwd	CAGATCCAGCCTCCAGCAAAC	75
	znhit3_exon4_rev	CATCCAGCAGATCCTCAACAGTC	
grip2a	grip2a_exon4_fwd	GCCATCCGCTTTATAGAGCCTG	72
	grip2a_exon5_rev	GAGAATTCTGTCGCCAACTTG	
slbp	slbp_exon1_fwd	CGATTACAAATCTAGTGAAGACAG	84
	slbp_exon2_rev	CTCAGAATACCATCTGCTCCAC	
tph1a	tph1a_exon6_fwd2	GAAGACAACATCCCTCAGCTG	77
	tph1a_exon7_rev2	GCCACAGGCCTGATGGTGAAG	
ntrk2b	ntrk2b_exon6_fwd	CTTAAATTCCAGCGAACACCC	83
	ntrk2b_exon7_rev	CATTTAGAGTCAGCACCGACTGC	
fgf1b	fgf1b_exon1_fwd	GCAATGGACAAATGTGGAAG	76
	fgf1b_exon2_rev	CCTCCATCTTCTCAATGAAGAAAC	

524 **Table S1. Primer sequences for qRT-PCR**. Gene names, primer names, sequences, and
525 product sizes are indicated.

METHODS

Zebrafish. Adult zebrafish of the Ekkwill, Tubingen, and AB strains were maintained at the Washington University Zebrafish Core Facility. All animal experiments were performed in compliance with institutional animal protocols. Male and female animals between 3 and 9 months of ~2 cm in length were used. Experimental fish and control siblings of similar size and equal sex distribution were used for all experiments. SC transection surgeries and regeneration analyses were performed in a blinded manner, and 2 to 4 independent experiments were repeated using different clutches of animals. The following previously published zebrafish strains were used: *mstn*^{bns5} (Dogra et al., 2017), Tg(*nes*:GFP) (Lam et al., 2009), Tg(*dbx1b*:GFP) (Satou et al., 2012), Tg(*slc6a5*:GFP) (McLean et al., 2007).

SC transection and treatment. Zebrafish were anaesthetized using MS-222. Fine scissors were used to make a small incision that transects the SC 4 mm caudal to the brainstem region. Complete transection was visually confirmed at the time of surgery. Injured animals were also assessed at 2 or 3 dpi to confirm loss of swim capacity post-surgery. For sham injuries, animals were anaesthetized, and fine scissors were used to transect skin and muscle tissues without inducing SCI.

For pro-MSTN treatment, lyophilized human MSTN proform peptide (BioVision, 4623P-10) was reconstituted in ddH_2O to a concentration 100 ng/μl. Zebrafish were anaesthetized using MS-222. 2 μl (200 ng) of reconstituted peptides were injected daily adjacent and lateral to the SC lesion site. 2 μl of ddH_2O was injected for vehicle controls.

For FGF1 treatment, lyophilized human FGF1 protein (PeproTech, 100-17A) was reconstituted in heparin to a concentration 250 ng/μl. Sterile Gelfoam Absorbable Gelatin Sponge (Pfizer, 09-0315-08) was cut into 2 mm^3 pieces, soaked with 2 μl of recombinant FGF1, then cut into 10 smaller pieces (50 ng per piece). Vehicle gelfoam pieces were soaked with 2 μl of heparin solution. At 5 dpi, zebrafish were anaesthetized using MS-222 and longitudinal incision lateral and parallel to the SC was made with fine scissors. Injured SC tissues were exposed without causing secondary injuries and gelfoam sponges were places adjacent to the lesion site. The incision was closed and glued using Vetbond tissue adhesive material as previously described (Mokalled et al., 2016).

554 **Bulk RNA sequencing.** Two mm SC sections, including the lesion site plus additional rostral and
555 caudal tissue proximal to the lesion, were collected from *mstnb* mutants and wild-type siblings at
556 1 wpi. Uninjured *mstnb* mutants and wild-type SCs were also collected. Total RNA was prepared
557 using NucleoSpin RNA Plus XS (Clontech, cat# 740990) and sent for bulk RNA sequencing.
558 TruSeq libraries were prepared and sequenced on Illumina HiSeq 3000 using 50 bp single-end
559 reading strategy. Quality QC and trimming of adapters and short sequences were performed
560 using Fastx. Sequencing reads were mapped to the zebrafish genome (Zv11) using Bowtie2, then
561 assembled and quantified using the Cufflinks and Cuffdiff algorithms. Genes with $\log_2$(fold
562 enrichment) between -1 and 1 or adjusted p-value ≥ 0.01 were considered insignificant. RNA
563 sequencing was performed at the Genome Technology Access Center at Washington University.
564 Analysis was performed in the Bioinformatics Core at the Center for Regenerative Medicine at
565 Washington University.

566 RNA-seq data (GEO accession number : GSE77025) was used to evaluate the expression of Tgf-
567 β ligands after complete SC transection. Log_2(fold change) is expressed for SCs at 1 wpi relative
568 to the sham injured SCs (Mokalled et al., 2016).

569 **Histology.** 16 µm µm cross cryosections of paraformaldehyde-fixed SC tissue were used. Tissue
570 sections were imaged using a Zeiss AxioVision compound microscope for *in situ* hybridization or
571 a Zeiss LSM 800 confocal microscope for immunofluorescence. *In situ* hybridization for *mstnb*
572 was performed as previously described (Mokalled et al., 2016).

573 For immunohistochemistry, tissue sections were rehydrated in PBT (0.1% Tween-20 in PBS),
574 then treated with blocking agent (5% goat serum in PBT) for 1 hr at room temperature. For nuclear
575 antigens, sections were treated with 0.2% TritonX-100 in PBT for 5 minutes and washed
576 thoroughly in PBT prior to the blocking step. Sections were incubated overnight with the indicated
577 primary antibodies, washed in PBT, and treated for 1 hr with secondary antibodies. Following
578 washes, sections were incubated in 1 mg/mL of Hoechst and mounted in Fluoromount-G
579 mounting media. Primary antibodies used in this study were: rabbit anti-Smad3(S423/425)
580 (Abcam, ab52903, 1:50), rabbit anti-PCNA (GeneTex, GTX124496, 1:500), mouse anti-HuC/D
581 (Invitrogen, A21271, 1:500), mouse anti-Gfap (ZIRC, Zrf1, 1:1000), mouse anti-acetylated α-
582 tubulin (Sigma, T6793, 1:1000), chicken anti-GFP (Aves Labs, 1020, 1:1000), rabbit anti-Sox2
583 (GeneTex, 124477, 1:250). Secondary antibodies (Invitrogen, 1:200) used in this study were

584 Alexa Fluor 488- or Alexa Fluor 594- conjugated goat anti-rabbit, anti-mouse, or anti-chicken
585 antibodies.

586 For simultaneous labeling with rabbit anti-Sox2 (GeneTex, 124477, 1:250) and rabbit anti-
587 pSmad3(S423/425) (abcam, ab52903, 1:50) (Fig. 1B), unconjugated Fab Fragment Goat Anti-
588 Rabbit IgG(H+L) (Jackson ImmunoResearch, 111-007-003) and donkey anti-goat 568 (Thermo
589 fisher: A-11057) antibodies were used for pSmad3 labeling. Sox2 was labeled using donkey anti-
590 rabbit-488 (Jackson ImmunoResearch, 711-547-003).

591 EdU Staining was adapted from a a previously described protocol (Salic and Mitchison, 2008).
592 Briefly, zebrafish were anaesthetized using MS-222 and subjected to intraperitoneal EdU
593 injections. 12.5 mM EdU (Sigma 900584) diluted in PBS was used. A single injection (Fig. 3 and
594 S2) or multiple, daily injections (Fig. 4 and S3) were performed and paraformaldehyde-fixed
595 cryosections were used. Sections were rehydrated in PBT for 10 min then incubated with freshly
596 prepared staining solution for 30 min (100 mM Tris (Sigma, T6066) pH 8.5; 1 mM $CuSO_4$ (Sigma,
597 C1297); 10 µM fluorescent azide; and 100 mM ascorbic acid (Sigma, A5960)).

598 **Cell counting.** Cell counting was performed using a customized Fiji script (adapting ITCN: Image
599 based Tool for counting nuclei- https://imagej.nih.gov/ij/plugins/itcn.html). Orthogonal projections
600 of individual image stacks were generated using Zen software. A Customized Fiji script
601 incorporated user-defined inputs to define channels (including Hoechst), to determine the center
602 of the central canal, and to outline SC perimeters. SC tissues dorsal to the central canal center
603 was considered “dorsal SC”. SC tissues ventral to the central canal center was considered
604 “ventral SC”. To quantify nuclei, the following parameters were set in ITCN counter: width, 15;
605 minimal distance, 7.5; threshold, 0.4. For each staining, thresholds were user-defined. Raw
606 counts from Fiji were processed using a customized R Studio script.

607 **Swim endurance assays.** Zebrafish were exercised in groups of 8-12 in a 5 L swim tunnel device
608 (Loligo, cat# SW100605L, 120V/60Hz). After 10 minutes of acclimation inside the enclosed
609 tunnel, water current velocity was increased every two minutes and fish swam against the current
610 until they reached exhaustion. Exhausted animals were removed from the chamber without
611 disturbing the remaining fish. Swim time and current velocity at exhaustion were recorded. Results
612 were expressed as means ± SEM. An unpaired two-tailed Student's t-test with Welch correction

was performed using the Prism software to determine statistical significance of swim times between groups.

Swim behavior assays. Zebrafish were divided into groups of 5 in a 5 L swim tunnel device (Loligo, cat# SW100605L, 120V/60Hz). Each group was allowed to swim for a total of 15 min under zero to low current velocities (5 min at 0 cm/s, 5 min at 10 cm/s, and 5 min at 15 cm/s). The entire swim behavior was recorded using high-speed camera (iDS, USB 3.0 color video camera) with following settings: aspect ratio, 1:4; pixel clock, 344; frame rate, 70 frames/s; exposure time: 0.29; aperture, 1.4 to 2; maximum frames; 63,000. Movies were converted to 20 frames/s and analyzed using a customized Fiji macro. For each frame, animals/objects > 1500 px^2 were identified, and the XY coordinates were derived for each animal/object. Frame were independently, and animal/object tracking was completed using a customized R Studio script. The script aligned coordinates, calculated swim metrics considering three separate frame windows (Frames 0-6000 at 0 cm/s; frames 6001-12000 at 10 cm/s, and frames 12001-18001 at 20 cm/s).

Glial bridging. GFAP immunohistochemistry was performed on serial transverse sections. The cross-sectional area of the glial bridge and the area of the intact SC rostral to the lesion were measured using ImageJ software. Bridging was calculated as a ratio of these measurements. Mann Whitney tests were performed using Prism software to determine statistical significance between groups.

Axon tracing. Anterograde axon tracing was performed on adult fish at 4 wpi. Fish were anaesthetized using MS-222 and fine scissors were used to transect the cord 4 mm rostral to the lesion site. Biocytin-soaked Gelfoam Gelatin Sponge was applied at the new injury site (Gelfoam, Pfizer, cat# 09-0315-08; Biocytin, saturated solution, Sigma, cat# B4261). Fish were euthanized 6 hours post-treatment and Biocytin was histologically detected using Alexa Fluor 594-conjugated Streptavidin (Molecular Probes, cat# S-11227). Biocytin-labeled axons were quantified using the “threshold” and “particle analysis” tools in the Fiji software. Four sections per fish at 0.5 (proximal) and 2 (distal) mm caudal to the lesion core, and 2 sections 1 mm rostral to the lesion, were analyzed. Axon growth was normalized to the efficiency of Biocytin labeling rostral to the lesion for each fish. The axon growth index was then normalized to the control group for each experiment. Mann-Whitney tests were performed using Prism software to determine statistical significance between groups

643 **Quantitative real time PCR.** Two mm SC sections, including the lesion site plus additional rostral
644 and caudal tissue proximal to the lesion, were collected for qRT-PCR. Total RNA was prepared
645 using NucleoSpin RNA Plus XS (Clontech, cat# 740990) and cDNA was synthesized using the
646 Maxima First Strand cDNA Synthesis Kit (ThermoFisher, cat# K1672) according to manufacturer's
647 specifications. Quantitative PCR was completed using the Luna polymerase master mix (NEB,
648 cat# M3003) using gene-specific primers (Table S1). Primers were designed to flank introns and
649 were confirmed to not amplify project from genomic DNA. To determine primer efficiency, a
650 standard curve was generated for each primer set using cDNA pooled from wild-type embryos at
651 1, 3, and 5 days post-fertilization. qRT-PCR was performed on a Bio-Rad CFX Connect Real-
652 Time System. For each gene, $\log_2$(fold change) was calculated using the DCq method and
653 normalized to *eif1a* as a loading control and to control gene expression for each experiment.

REFERENCES

Adolf, B., Chapouton, P., Lam, C., Topp, S., Tannhäuser, B., Strähle, U., Götz, M., and Bally-Cuif, L. (2006). Conserved and acquired features of adult neurogenesis in the zebrafish telencephalon. Developmental biology *295*.

Alizadeh, A., Dyck, S., and Karimi-Abdolrezaee, S. (2019). Traumatic Spinal Cord Injury: An Overview of Pathophysiology, Models and Acute Injury Mechanisms. Frontiers in neurology *10*.

Bagheri-Mohammadi, S. (2021). Adult neurogenesis and the molecular signalling pathways in brain: the role of stem cells in adult hippocampal neurogenesis. Int J Neurosci, 1-13.

Barbosa, J., Sanchez-Gonzalez, R., Di Giaimo, R., Baumgart, E., Theis, F., Götz, M., and Ninkovic, J. (2015). Neurodevelopment. Live imaging of adult neural stem cell behavior in the intact and injured zebrafish brain. Science (New York, NY) *348*.

Barnabe-Heider, F., Goritz, C., Sabelstrom, H., Takebayashi, H., Pfrieger, F.W., Meletis, K., and Frisen, J. (2010). Origin of new glial cells in intact and injured adult spinal cord. Cell Stem Cell *7*, 470-482.

Barreiro-Iglesias, A., Mysiak, K.S., Scott, A.L., Reimer, M.M., Yang, Y., Becker, C.G., and Becker, T. (2015). Serotonin Promotes Development and Regeneration of Spinal Motor Neurons in Zebrafish. Cell Rep *13*, 924-932.

Becker, T., Bernhardt, R., Reinhard, E., Wullimann, M., Tongiorg, i.E., and Schachner, M. (1998). Readiness of zebrafish brain neurons to regenerate a spinal axon correlates with differential expression of specific cell recognition molecules. The Journal of neuroscience : the official journal of the Society for Neuroscience *18*.

Becker, T., Wullimann, M., Becker, C., Bernhardt, R., and Schachner, M. (1997). Axonal regrowth after spinal cord transection in adult zebrafish. The Journal of comparative neurology *377*.

Chapouton, P., Skupien, P., Hesl, B., Coolen, M., Moore, J., Madelaine, R., Kremmer, E., Faus-Kessler, T., Blader, P., Lawson, N.*, et al.* (2010). Notch activity levels control the balance between quiescence and recruitment of adult neural stem cells. The Journal of neuroscience : the official journal of the Society for Neuroscience *30*.

Dogra, D., Ahuja, S., Kim, H.T., Rasouli, S.J., Stainier, D.Y.R., and Reischauer, S. (2017). Opposite effects of Activin type 2 receptor ligands on cardiomyocyte proliferation during development and repair. Nat Commun *8*, 1902.

Goldshmit, Y., Sztal, T.E., Jusuf, P.R., Hall, T.E., Nguyen-Chi, M., and Currie, P.D. (2012). Fgf-dependent glial cell bridges facilitate spinal cord regeneration in zebrafish. J Neurosci *32*, 7477-7492.

686 Grandel, H., Kaslin, J., Ganz, J., Wenzel, I., and Brand, M. (2006). Neural stem cells and
687 neurogenesis in the adult zebrafish brain: origin, proliferation dynamics, migration and cell fate.
688 Developmental biology *295*.

689 Hachem, L., Ahuja, C., and Fehlings, M. (2017). Assessment and management of acute spinal cord
690 injury: From point of injury to rehabilitation. The journal of spinal cord medicine *40*.

691 Hinckley, C., Seebach, B., and Ziskind-Conhaim, L. (2005). Distinct roles of glycinergic and
692 GABAergic inhibition in coordinating locomotor-like rhythms in the neonatal mouse spinal cord.
693 Neuroscience *131*.

694 Horky, L.L., Galimi, F., Gage, F.H., and Horner, P.J. (2006). Fate of endogenous stem/progenitor
695 cells following spinal cord injury. J Comp Neurol *498*, 525-538.

696 Horner, P.J., Power, A.E., Kempermann, G., Kuhn, H.G., Palmer, T.D., Winkler, J., Thal, L.J.,
697 and Gage, F.H. (2000). Proliferation and differentiation of progenitor cells throughout the intact
698 adult rat spinal cord. J Neurosci *20*, 2218-2228.

699 Hsu, Y., Lee, D., Chen, S., Liao, W., Lin, J., Chiu, W., and Chiu, I. (2009). Brain-specific 1B
700 promoter of FGF1 gene facilitates the isolation of neural stem/progenitor cells with self-renewal
701 and multipotent capacities. Developmental dynamics : an official publication of the American
702 Association of Anatomists *238*.

703 Jovanović, K., Petrov, T., and Stein, R. (1999). Effects of inhibitory neurotransmitters on the
704 mudpuppy (Necturus maculatus) locomotor pattern in vitro. Experimental brain research *129*.

705 Kambadur, R., Sharma, M., Smith, T.P., and Bass, J.J. (1997). Mutations in myostatin (GDF8) in
706 double-muscled Belgian Blue and Piedmontese cattle. Genome Res *7*, 910-916.

707 Keatinge, M., Tsarouchas, T.M., Munir, T., Porter, N.J., Larraz, J., Gianni, D., Tsai, H.H., Becker,
708 C.G., Lyons, D.A., and Becker, T. (2021). CRISPR gRNA phenotypic screening in zebrafish
709 reveals pro-regenerative genes in spinal cord injury. PLoS Genet *17*, e1009515.

710 Kerrison, J.B., Lewis, R.N., Otteson, D.C., and Zack, D.J. (2005). Bone morphogenetic proteins
711 promote neurite outgrowth in retinal ganglion cells. Mol Vis *11*, 208-215.

712 Klatt Shaw, D., and Mokalled, M.H. (2021). Efficient CRISPR/Cas9 mutagenesis for
713 neurobehavioral screening in adult zebrafish. G3 (Bethesda).

714 Klatt Shaw, D., Saraswathy, V.M., Zhou, L., McAdow, A.R., Burris, B., Butka, E., Morris, S.A.,
715 Dietmann, S., and Mokalled, M.H. (2021). Localized EMT reprograms glial progenitors to
716 promote spinal cord repair. Dev Cell *56*, 613-626 e617.

717 Kroehne, V., Freudenreich, D., Hans, S., Kaslin, J., and Brand, M. (2011). Regeneration of the
718 adult zebrafish brain from neurogenic radial glia-type progenitors. Development (Cambridge,
719 England) *138*.

720 Kuscha, V., Frazer, S., Dias, T., Hibi, M., Becker, T., and Becker, C. (2012a). Lesion-induced
721 generation of interneuron cell types in specific dorsoventral domains in the spinal cord of adult
722 zebrafish. The Journal of comparative neurology *520*.

723 Kuscha, V., Frazer, S.L., Dias, T.B., Hibi, M., Becker, T., and Becker, C.G. (2012b). Lesion-
724 induced generation of interneuron cell types in specific dorsoventral domains in the spinal cord of
725 adult zebrafish. J Comp Neurol *520*, 3604-3616.

726 Lam, C., März, M., and Strähle, U. (2009). gfap and nestin reporter lines reveal characteristics of
727 neural progenitors in the adult zebrafish brain. Developmental dynamics : an official publication
728 of the American Association of Anatomists *238*.

729 Langley, B., Thomas, M., Bishop, A., Sharma, M., Gilmour, S., and Kambadur, R. (2002).
730 Myostatin inhibits myoblast differentiation by down-regulating MyoD expression. J Biol Chem
731 *277*, 49831-49840.

732 Le, W., and Yao, J. (2017). The Effect of Myostatin (GDF-8) on Proliferation and Tenocyte
733 Differentiation of Rat Bone Marrow-Derived Mesenchymal Stem Cells. The journal of hand
734 surgery Asian-Pacific volume *22*.

735 Li, L., and Clevers, H. (2010). Coexistence of quiescent and active adult stem cells in mammals.
736 Science *327*, 542-545.

737 Li, S., Gu, X., and Yi, S. (2017). The Regulatory Effects of Transforming Growth Factor-β on
738 Nerve Regeneration. Cell transplantation *26*.

739 Lim, S., McMahon, C., Matthews, K., Devlin, G., Elston, M., and Conaglen, J. (2018). Absence
740 of Myostatin Improves Cardiac Function Following Myocardial Infarction. Heart, lung &
741 circulation *27*.

742 Magga, J., Vainio, L., Kilpio, T., Hulmi, J.J., Taponen, S., Lin, R., Rasanen, M., Szabo, Z., Gao,
743 E., Rahtu-Korpela, L.*, et al.* (2019). Systemic Blockade of ACVR2B Ligands Protects
744 Myocardium from Acute Ischemia-Reperfusion Injury. Mol Ther *27*, 600-610.

745 März, M., Chapouton, P., Diotel, N., Vaillant, C., Hesl, B., Takamiya, M., Lam, C., Kah, O., Bally-
746 Cuif, L., and Strähle, U. (2010). Heterogeneity in progenitor cell subtypes in the ventricular zone
747 of the zebrafish adult telencephalon. Glia *58*.

748 Massagué, J. (2012). TGFβ signalling in context. Nature reviews Molecular cell biology *13*.

749 McCroskery, S., Thomas, M., Maxwell, L., Sharma, M., and Kambadur, R. (2003). Myostatin
750 negatively regulates satellite cell activation and self-renewal. J Cell Biol *162*, 1135-1147.

751 McCroskery, S., Thomas, M., Platt, L., Hennebry, A., Nishimura, T., McLeay, L., Sharma, M.,
752 and Kambadur, R. (2005). Improved muscle healing through enhanced regeneration and reduced
753 fibrosis in myostatin-null mice. J Cell Sci *118*, 3531-3541.

754 McLean, D., Fan, J., Higashijima, S., Hale, M., and Fetcho, J. (2007). A topographic map of
755 recruitment in spinal cord. Nature *446*.

756 Meletis, K., Barnabe-Heider, F., Carlen, M., Evergren, E., Tomilin, N., Shupliakov, O., and Frisen,
757 J. (2008). Spinal cord injury reveals multilineage differentiation of ependymal cells. PLoS Biol *6*,
758 e182.

759 Mokalled, M.H., Patra, C., Dickson, A.L., Endo, T., Stainier, D.Y., and Poss, K.D. (2016). Injury-
760 induced ctgfa directs glial bridging and spinal cord regeneration in zebrafish. Science *354*, 630-
761 634.

762 Muthusamy, N., Brumm, A., Zhang, X., Carmichael, S.T., and Ghashghaei, H.T. (2018). Foxj1
763 expressing ependymal cells do not contribute new cells to sites of injury or stroke in the mouse
764 forebrain. Sci Rep *8*, 1766.

765 Ogai, K., Nakatani, K., Hisano, S., Sugitani, K., Koriyama, Y., and Kato, S. (2014). Function of
766 Sox2 in ependymal cells of lesioned spinal cords in adult zebrafish. Neuroscience research *88*.

767 Oyinbo, C. (2011). Secondary injury mechanisms in traumatic spinal cord injury: a nugget of this
768 multiply cascade. Acta neurobiologiae experimentalis *71*.

769 Pierani, A., Moran-Rivard, L., Sunshine, M., Littman, D., Goulding, M., and Jessell, T. (2001).
770 Control of interneuron fate in the developing spinal cord by the progenitor homeodomain protein
771 Dbx1. Neuron *29*.

772 Reimer, M., Kuscha, V., Wyatt, C., Sörensen, I., Frank, R., Knüwer, M., Becker, T., and Becker,
773 C. (2009). Sonic hedgehog is a polarized signal for motor neuron regeneration in adult zebrafish.
774 The Journal of neuroscience : the official journal of the Society for Neuroscience *29*.

775 Reimer, M.M., Norris, A., Ohnmacht, J., Patani, R., Zhong, Z., Dias, T.B., Kuscha, V., Scott, A.L.,
776 Chen, Y.C., Rozov, S.*, et al.* (2013). Dopamine from the brain promotes spinal motor neuron
777 generation during development and adult regeneration. Dev Cell *25*, 478-491.

778 Reimer, M.M., Sorensen, I., Kuscha, V., Frank, R.E., Liu, C., Becker, C.G., and Becker, T. (2008).
779 Motor neuron regeneration in adult zebrafish. The Journal of neuroscience : the official journal of
780 the Society for Neuroscience *28*, 8510-8516.

781 Ren, Y., Ao, Y., O'Shea, T.M., Burda, J.E., Bernstein, A.M., Brumm, A.J., Muthusamy, N.,
782 Ghashghaei, H.T., Carmichael, S.T., Cheng, L.*, et al.* (2017). Ependymal cell contribution to scar
783 formation after spinal cord injury is minimal, local and dependent on direct ependymal injury. Sci
784 Rep *7*, 41122.

785 Rodgers, B.D., Wiedeback, B.D., Hoversten, K.E., Jackson, M.F., Walker, R.G., and Thompson,
786 T.B. (2014). Myostatin stimulates, not inihibits, C2C12 myoblast proliferation. Endocrinology
787 *155*, 670-675.

788 Rothenaigner, I., Krecsmarik, M., Hayes, J., Bahn, B., Lepier, A., Fortin, G., Götz, M., Jagasia,
789 R., and Bally-Cuif, L. (2011). Clonal analysis by distinct viral vectors identifies bona fide neural
790 stem cells in the adult zebrafish telencephalon and characterizes their division properties and fate.
791 Development (Cambridge, England) *138*.

792 Salic, A., and Mitchison, T. (2008). A chemical method for fast and sensitive detection of DNA
793 synthesis in vivo. Proceedings of the National Academy of Sciences of the United States of
794 America *105*.

795 Sartori, R., Gregorevic, P., and Sandri, M. (2014). TGFβ and BMP signaling in skeletal muscle:
796 potential significance for muscle-related disease. Trends in endocrinology and metabolism: TEM
797 *25*.

798 Satou, C., Kimura, Y., and Higashijima, S. (2012). Generation of multiple classes of V0 neurons
799 in zebrafish spinal cord: progenitor heterogeneity and temporal control of neuronal diversity. The
800 Journal of neuroscience : the official journal of the Society for Neuroscience *32*.

801 Schuelke, M., Wagner, K.R., Stolz, L.E., Hubner, C., Riebel, T., Komen, W., Braun, T., Tobin,
802 J.F., and Lee, S.J. (2004). Myostatin mutation associated with gross muscle hypertrophy in a child.
803 N Engl J Med *350*, 2682-2688.

804 Shah, P.T., Stratton, J.A., Stykel, M.G., Abbasi, S., Sharma, S., Mayr, K.A., Koblinger, K.,
805 Whelan, P.J., and Biernaskie, J. (2018). Single-Cell Transcriptomics and Fate Mapping of
806 Ependymal Cells Reveals an Absence of Neural Stem Cell Function. Cell *173*, 1045-1057 e1049.

807 Sharma, M., McFarlane, C., Kambadur, R., Kukreti, H., Bonala, S., and Srinivasan, S. (2015).
808 Myostatin: expanding horizons. IUBMB life *67*.

809 Sibilla, S., and Ballerini, L. (2009). GABAergic and glycinergic interneuron expression during
810 spinal cord development: dynamic interplay between inhibition and excitation in the control of
811 ventral network outputs. Progress in neurobiology *89*.

812 Silva, N., Sousa, N., Reis, R., and Salgado, A. (2014). From basics to clinical: a comprehensive
813 review on spinal cord injury. Progress in neurobiology *114*.

814 Singh, A., Tetreault, L., Kalsi-Ryan, S., Nouri, A., and Fehlings, M. (2014). Global prevalence
815 and incidence of traumatic spinal cord injury. Clinical epidemiology *6*.

816 Sofroniew, M.V. (2018). Dissecting spinal cord regeneration. Nature *557*, 343-350.

817 Taylor, W.E., Bhasin, S., Artaza, J., Byhower, F., Azam, M., Willard, D.H., Jr., Kull, F.C., Jr., and
818 Gonzalez-Cadavid, N. (2001). Myostatin inhibits cell proliferation and protein synthesis in C2C12
819 muscle cells. Am J Physiol Endocrinol Metab *280*, E221-228.

820 Than-Trong, E., Kiani, B., Dray, N., Ortica, S., Simons, B., Rulands, S., Alunni, A., and Bally-
821 Cuif, L. (2020). Lineage hierarchies and stochasticity ensure the long-term maintenance of adult
822 neural stem cells. Science advances *6*.

823 Than-Trong, E., Ortica-Gatti, S., Mella, S., Nepal, C., Alunni, A., and Bally-Cuif, L. (2018).
824 Neural stem cell quiescence and stemness are molecularly distinct outputs of the Notch3 signalling
825 cascade in the vertebrate adult brain. Development (Cambridge, England) *145*.

826 Tran, A.P., Warren, P.M., and Silver, J. (2021). New insights into glial scar formation after spinal
827 cord injury. Cell Tissue Res.

828 Uribe, V., Ramadass, R., Dogra, D., Rasouli, S.J., Gunawan, F., Nakajima, H., Chiba, A.,
829 Reischauer, S., Mochizuki, N., and Stainier, D.Y.R. (2018). In vivo analysis of cardiomyocyte
830 proliferation during trabeculation. Development *145*.

831 Wallner, C., Jaurich, H., Wagner, J., Becerikli, M., Harati, K., Dadras, M., Lehnhardt, M., and
832 Behr, B. (2017). Inhibition of GDF8 (Myostatin) accelerates bone regeneration in diabetes mellitus
833 type 2. Scientific reports *7*.

834 Whittemore, L.A., Song, K., Li, X., Aghajanian, J., Davies, M., Girgenrath, S., Hill, J.J., Jalenak,
835 M., Kelley, P., Knight, A.*, et al.* (2003). Inhibition of myostatin in adult mice increases skeletal
836 muscle mass and strength. Biochem Biophys Res Commun *300*, 965-971.

837 Wu, H.H., Ivkovic, S., Murray, R.C., Jaramillo, S., Lyons, K.M., Johnson, J.E., and Calof, A.L.
838 (2003). Autoregulation of neurogenesis by GDF11. Neuron *37*, 197-207.

839 Yamamoto, S., Yamamoto, N., Kitamura, T., Nakamura, K., and Nakafuku, M. (2001).
840 Proliferation of parenchymal neural progenitors in response to injury in the adult rat spinal cord.
841 Exp Neurol *172*, 115-127.

842 Zhu, X., Hadhazy, M., Wehling, M., Tidball, J., and McNally, E. (2000). Dominant negative
843 myostatin produces hypertrophy without hyperplasia in muscle. FEBS letters *474*.